JBC Papers in Press. Published on April 16, 2015 as Manuscript M115.650523
The latest version is at http://www.jbc.org/cgi/doi/10.1074/jbc.M115.650523

Interaction of the *Clostridium difficile* Binary Toxin CDT and its Host Cell Receptor LSR*

Sarah Hemmasi[1,2,$], Bernd A. Czulkies[1,3,$], Björn Schorch[1,2,4], Antonia Veit[1], Klaus Aktories[1,5], and Panagiotis Papatheodorou[1]

From the [1]Institut für Experimentelle und Klinische Pharmakologie und Toxikologie, [2]Fakultät für Biologie, [3]Hermann Staudinger Graduate School (HSGS), [4]Spemann Graduate School of Biology and Medicine (SGBM), and [5]Centre for Biological Signalling Studies (BIOSS), Albert-Ludwigs-Universität Freiburg, D-79104 Freiburg, Germany

*Running title: *Interaction of CDT and LSR*

To whom correspondence should be addressed: Panagiotis Papatheodorou, Institut für Experimentelle und Klinische Pharmakologie und Toxikologie, Albert-Ludwigs-Universität Freiburg, Alberstr. 25, D-79104 Freiburg, Tel.: +49(0)761-2035308; Fax: (+49(0)761-2035311; E-mail: panagiotis.papatheodorou@pharmakol.uni-freiburg.de

Keywords: Bacterial toxin, protein-protein interaction, receptor, immunoglobulin-like domain, gene knockout, *Clostridium difficile* infection; toxin uptake

Background: *Clostridium difficile* binary toxin CDT enters host cells via its receptor LSR.
Results: Regions responsible for the CDT-LSR interaction were identified.
Conclusion: An immunoglobulin-like domain of LSR and amino acids 757 to 866 of the binding component of CDT determine the toxin-receptor interaction.
Significance: Knowledge of the toxin-receptor interaction is key to the development of anti-toxin strategies.

ABSTRACT

CDT (*Clostridium difficile* transferase) is a binary, actin ADP-ribosylating toxin frequently associated with hypervirulent strains of the human enteric pathogen *C. difficile*, the most serious cause of antibiotic-associated diarrhea and pseudomembranous colitis. CDT leads to the collapse of the actin cytoskeleton and, eventually, to cell death. Low doses of CDT result in the formation of microtubule-based protrusions on the cell surface that increases the adherence and colonization of *C. difficile*. The lipolysis-stimulated lipoprotein receptor (LSR) is the host cell receptor for CDT and our aim was to gain a deeper insight into the interplay between both proteins. We show that CDT interacts with the extracellular, Ig-like domain of LSR with an affinity in the nanomolar range. We identified LSR splice variants in the colon carcinoma cell line HCT116 and disrupted the LSR gene in these cells by applying the CRISPR-Cas9 technology. LSR truncations ectopically expressed in LSR knockout cells indicated that intracellular parts of LSR are not essential for plasma membrane targeting of the receptor and cellular uptake of CDT. By generating a series of N- and C-terminal truncations of the binding component of CDT (CDTb), we found that amino acids 757 to 866 of CDTb are sufficient for binding to LSR. With a transposon-based, random mutagenesis approach we identified potential LSR-interacting epitopes in CDTb. This study increases our understanding about the interaction between CDT and its receptor LSR, which is key to the development of anti-toxin strategies for preventing cell entry of the toxin.

Clostridium difficile is a human enteric pathogen and the most serious cause of antibiotic-associated diarrhea and pseudomembranous colitis (1-3). In recent years, hypervirulent strains of the pathogen have caused epidemics in developed countries that were associated with more severe disease and increased death rates (4-7). One hallmark of hypervirulent *C. difficile* strains, such as the BI/Nap1/027, is the production of a third toxin, the *Clostridium difficile* transferase (CDT)[6], in addition to the Rho-glucosylating toxins A and B (8,9).

CDT belongs to the family of clostridial ADP-ribosylating toxins, exhibiting the highest similarity

Copyright 2015 by The American Society for Biochemistry and Molecular Biology, Inc.

Downloaded from http://www.jbc.org/ at Shanghai Information Center for Life Sciences, Chinese Academy of Sciences on May 25, 2015

to members of the subfamily of iota-like toxins, which includes the eponym *Clostridium perfringens* iota-toxin and the *Clostridium spiroforme* toxin (CST) (9,10). CDT consists of two components, a biologically active enzyme component (CDTa) and a separate binding component (CDTb). At first, CDTb interacts with a host receptor on the cell surface. Before or after this step, CDTb undergoes proteolytic activation to form a heptameric prepore already in solution or at the cell surface, respectively. After binding of CDTa to the prepore-receptor complex, the toxin reaches endosomal compartments via receptor-mediated endocytosis. Acidification of the endosomal lumen triggers conformational changes within the prepore, resulting in membrane insertion and subsequent pore formation (11-14). By the guidance of cytosolic chaperones, CDTa then translocates through the pore into the cytosol, where it ADP-ribosylates G-actin at arginine-177, thereby causing actin depolymerization and, eventually, cell death (9,15-18). However, at low doses of the toxin, destruction of the cortical actin results in the formation of microtubule-based protrusions on epithelial cells that increase the adherence and colonization of *C. difficile* (19).

Using a haploid genetic screen, we recently identified the lipolysis-stimulated lipoprotein receptor (LSR) as the host cell receptor for all members of the iota-toxin family, including CDT (20-22). LSR is a type I, single-pass, transmembrane protein, featuring an immunoglobulin (Ig)-like V-type domain in the extracellular part of the protein. The receptor is mainly expressed in the liver, but also in the intestine and various other tissues (23-25). Initially, LSR was identified as a hepatic receptor for triglyceride-rich lipoproteins (26,27). More recently, LSR was found to act in the recruitment of tricellulin to tricellular contacts that are important for the integrity of epithelial barriers (28,29).

In the present study we obtained binding kinetics of CDT and LSR and identified regions in both proteins that determine their interaction. We show with recombinant proteins that the extracellular, Ig-like domain of LSR provides the platform for the binding of CDT. Furthermore, we generated an HCT116 LSR knockout cell line and ectopically expressed LSR truncations to clarify whether intracellular parts of LSR are required for plasma membrane targeting of the receptor and endocytic uptake of CDT. The receptor-binding domain (RBD) of CDT has only been roughly localized at the C-terminus of CDTb. To narrow down this region, we generated a series of N- and C-terminal truncations of the RBD of CDTb and tested them for binding to LSR. Additionally, we applied transposon-based, random mutagenesis to the RBD of CDTb to identify epitopes potentially involved in the interaction with LSR.

EXPERIMENTAL PROCEDURES

Generation, transfection, and cultivation of mammalian cells – All mammalian cells used in this study were grown in DMEM (12 mM L-glutamine) supplemented with 10% (vol/vol) FCS, 1% (vol/vol) non-essential amino acids, 1% (vol/vol) sodium pyruvate, and 1% (vol/vol) penicillin/streptomycin, and incubated at 37°C with 5% (vol/vol) CO_2 under humidified conditions. Transfections were performed either with PEI (polyethylenimine) or with peqFECT transfection reagent (PeqLab) according to the manufacturer´s protocol. If necessary, cells were co-transfected with an EGFP-expressing plasmid (pEGFP-N1; Clontech) to visualize the transfected cells with fluorescence microscopy.

HCT116 LSR knockout cells were generated via the CRISPR-Cas9 technology and by following the recently established protocol from the Church laboratory (30). Briefly, a gRNA expression fragment was ordered as a gBlock (Integrated DNA Technologies, Leuven, Belgium) that consisted of an U6 promoter followed by a 20 bp protospacer, a PAM (protospacer adjacent motif) sequence, and a scaffold and terminator sequence. The protospacer sequence (5´-GGACAGCGTGCGCACCGTCA-3´) was complementary to a sequence in exon 2 of the LSR gene. The gBlock was then inserted into the pCR-Blunt II-TOPO vector and the resulting plasmid transfected into HCT116 cells together with the human codon-optimized Cas9 expression plasmid pcDNA3.3-TOPO/hCas9 (Addgene plasmid #41815). Transfected cells were first grown under antibiotic selection pressure with neomycin and then treated with CDT for the selection of toxin-resistant HCT116 LSR knockout cells. Finally, a single HCT116 LSR knockout clone was isolated via limiting dilution cloning and named $HCT116_{\Delta LSR}$. A base pair insertion in exon 2 of the LSR gene of $HCT116_{\Delta LSR}$ cells, resulting in a frame-shift mutation, could be confirmed by PCR and Sanger sequencing of the genomic region flanking the mutation site.

Downloaded from http://www.jbc.org/ at Shanghai Information Center for Life Sciences, Chinese Academy of Sciences on May 25, 2015

H1-HeLa(+LSR) cells were obtained by transducing H1-HeLa cells with a FLAG-LSR-expressing retrovirus as described previously (20) and the same procedure was applied for the transduction of $HCT116_{\Delta LSR}$ cells with a FLAG- or FLAG-LSR-expressing retrovirus to generate $HCT116_{\Delta LSR}$(+FLAG) and $HCT116_{\Delta LSR}$(+FLAG-LSR) cells.

Cloning, mutagenesis, recombinant proteins, and source of toxins – For the recombinant expression and purification of the Ig-like domain of human LSR, a DNA fragment encoding amino acids 39-192 of the LSR protein (referring to the LSR variant with the accession number AAH04381.2) was amplified by PCR with oligonucleotides generating a 5´-NcoI and a 3´-HindIII restriction site and by using the previously described plasmid pMXs-IRES-Blasticidin/FLAG-LSR as template (20). The PCR product was then ligated into an NcoI/HindIII-opened pET28a vector to generate pET28a/LSR_{Ig}-His6. The resulting plasmid was then transformed into *Escherichia coli* strain BL21 (DE3). Transformants were grown in LB medium at 37°C until an optical density at 600 nm (OD_{600}) of 0.4 to 0.6 was reached and then protein expression was induced by the addition of 0.2 mM isopropyl-β-D-thiogalactopyranoside (IPTG) and overnight incubation at 21°C. The next day, the cells were harvested by centrifugation (5,000 g, 20 min, 4°C) and resuspended in lysis buffer (20 mM Tris-HCl/pH 8, 300 mM NaCl, and 0.5 mM EDTA) complemented with 1 mM PMSF and 5 µg/ml DNase, prior to lysis of the cells by the use of a microfluidizer at 15,000 lb/in^2. Following centrifugation (14,000 g, 30 min, 4°C) of the cell lysate, the supernatant was discarded and the pellet further processed for purification of LSR_{Ig}-His6 from inclusion bodies. In order to obtain purified inclusion bodies, the pellet was resuspended in washing buffer (lysis buffer including 1% (wt/vol) Triton X-100 and 10 mM DTT) and then briefly sonicated (3x30 sec, 80% power, 70% duty cycle; Bandelin Sonopuls HD 60), prior to centrifugation (14,000 g, 20 min, 4°C) to precipitate again the inclusion bodies. This washing step was performed twice and then once again with washing buffer without Triton X-100. Next, the inclusion bodies were resuspended in solubilisation buffer (20 mM Tris-HCl/pH 8, 500 mM NaCl, and 5 mM DTT) complemented with 6 M urea, sonicated (3x30 sec, 80% power, 70% duty cycle) and incubated overnight at 4°C under gentle rotation. Non-solubilised material was removed by centrifugation (14,000 g, 30 min, 4°C) and the supernatant dialysed at 4°C overnight first against the 75-fold volume of refolding buffer (20 mM Tris-HCl/pH 8, 150 mM NaCl, 0.3 M L-arginine, 10 mM reduced glutathione, and 5 mM oxidized glutathione) and a second time against the 125-fold volume of storage buffer (150 mM Tris-HCl/pH 8, and 20 mM NaCl).

The plasmid pEGFP-N1/LSR was used for the ectopic expression of LSR-EGFP in mammalian cells and is described elsewhere (31). The pEGFP-N1 vector backbone was also used for the ectopic expression of LSR_{1-240}-EGFP and $LSR_{\Delta CR}$-EGFP. Cloning of these two constructs was performed as follows: a DNA fragment encoding LSR_{1-240} was generated by PCR amplification of the respective region, whereas LSR with deletion of the cysteine-rich region was generated via overlap extension PCR; in both cases primers were used that generated a 5´-NheI and a 3´-HindIII restriction site for ligation into a NheI/HindIII-opened pEGFP-N1 vector to finally obtain pEGFP-N1/LSR_{1-240} and pEGFP-N1/$LSR_{\Delta CR}$, respectively. Eventually, all LSR constructs were subcloned with identical restriction sites into the ptdTomato-N1 backbone for ectopic expression of LSR-, LSR_{1-240}, and $LSR_{\Delta CR}$-Tomato in mammalian cells.

Plasmids for the expression of mLSR, mILDR1, and mILDR2 in mammalian cells were kindly provided by Mikio Furuse (Kobe University, Japan) and are described elsewhere (29,32).

The plasmid pcDNA3-dsRed-ER (contains the N-terminal endoplasmic reticulum (ER) targeting sequence of calreticulin and a C-terminal KDEL ER retention sequence) was kindly shared by Llewelyn Roderick (Cambridge, UK) and was used for ER colocalization studies.

CDTa and the precursor form of CDTb (pCDTb) were purified as recombinant proteins from the expression host *Bacillus megaterium* with protocols described earlier (33). CDTb was obtained by proteolytic activation of pCDTb (11,34). If not otherwise stated, 1 nM CDTa together with 0.2 nM CDTb were added to cultured cells for intoxication experiments.

The cloning, expression and purification of the receptor-binding domain (RBD) of CDTb as a glutathione-S-transferase (GST) fusion protein (GST-RBD) has been decribed elsewhere (31). N- and C-terminal truncations of RBD were expressed and purified from *Escherichia coli* strain BL21 (DE3) as GST fusion proteins in the same manner

Downloaded from http://www.jbc.org/ at Shanghai Information Center for Life Sciences, Chinese Academy of Sciences on May 25, 2015

as GST-RBD. The expression plasmids for the RBD truncations were generated by amplifying the corresponding sequence of the RBD by PCR with primers generating a 5´-EcoRI and a 3´-XhoI restriction site and by using pGEX-4T3/RBD (31) as template. The PCR products were then ligated into an EcoRI/XhoI-opened pGEX-4T3. The pGEX-4T3/RBD plasmid was also used as template to generate transposon-based RBD mutants with the MGS™ Mutation Generation System (Thermo Scientific) following the manufacturer´s protocol.

Analysis of cell surface-binding of DyLight-labeled proteins by flow cytometry – DyLight 488 NHS ester (Thermo Scientific) was coupled to purified proteins in phosphate-buffered saline (PBS) including 10% (w/v) glycerol following the manufacturer´s instructions. Micro Bio-Spin 6 columns (Bio-Rad Laboratories) were used to remove excess dye after the labeling reaction.

To analyze cell surface binding of DyLight-labeled proteins, cells from the mammalian cell line of interest were first detached from culture plates with PBS complemented with 10 mM EDTA, then washed twice with PBS, and kept on ice. Typically, 3 x 10^5 cells were incubated with the indicated amounts of DyLight-labeled proteins for 10 min in 0.1 ml DMEM medium on ice. For competition studies, non-labeled proteins were preincubated with cells for 10 min on ice, prior to the addition of the DyLight-labeled protein. The cells were then washed twice with PBS and subjected to flow cytometric analysis using the BD FACSCalibur platform. Cell surface-bound fluorescence was detected with an argon-ion laser (488 nm) and a 530-nm-bandpass filter (FITC). For multicolor FACS measurements the BD FACSCANTO II platform was used. Flowing Software (version 2.5.0) was used for the computational analysis of the FACS measurements.

Surface plasmon resonance measurements – Dynamic interactions of GST-RBD with the immunoglobulin-like domain of LSR were analyzed using a Biacore X100 system (Biacore). LSR_{Ig} (25 µg/mL in 10 mM sodium acetate, pH 4.0) was amine-coupled on a CM5 sensor chip according to the manufacturer's instructions, achieving approximately 3,000 response units (RU). Sensograms were performed in binding buffer (10 mM HEPES, 150 mM NaCl, and 0.05% Tween-20, pH 7.4) at 25°C with a flow rate of 30 µL/min. Up to 5 increasing concentrations of putative protein ligand were injected per cycle for 120 sec and dissociation was allowed for 600 sec. The chip surface was regenerated at the beginning of each binding cycle by sequential flux of two buffers, containing (a) 1 M NaCl and 10 mM sodium acetate (pH 4.0) and (b) 1 M NaCl, and 10 mM NaOH, with each flux lasting 90 seconds. Kinetic constants were calculated using the Biacore X100 Evaluation Software (V 2.0).

Immunoblot analysis – For the detection of LSR a rabbit polyclonal anti-LSR antibody (clone X-25) (sc-133765; Santa Cruz) was used. His- and GST-tagged proteins were detected with rabbit polyclonal anti-His (#2365; Cell Signaling Technology) and mouse monoclonal anti-GST (sc-138; Santa Cruz) antibodies, respectively. Sodium-potassium-transporting ATPase subunit alpha-1 (ATP1A1) was detected with mouse monoclonal anti-ATP1A1 antibody (ab7671; Abcam). Tubulin was detected with mouse monoclonal anti-tubulin antibody (T9026; Sigma-Aldrich). Rabbit monoclonal anti-GFP (#2956; Cell Signaling Technology) antibody was used to detect EGFP fusion proteins. Horseradish peroxidase-conjugated donkey anti-mouse IgG (H&L) (#610-703-124; Rockland) or goat anti-rabbit IgG (H&L) (#7074; Cell Signaling) antibodies were used as secondary antibodies. Antibody signals were developed by the enhanced chemiluminescence reaction and quantified with MultiGauge software (FujiFilm).

Microscopy – Morphological changes of cultured cells after intoxication with CDT were analyzed directly in wells by using an inverted light microscope (Axiovert 25, Carl Zeiss). Images were obtained with an inbuilt digital camera (AxioCam HRc). Fluorescence microscopy was performed with an inverted stage manual fluorescent microscope (Axiovert 35M; Carl Zeiss) equipped with standard filters and an AxioCam HRm (Carl Zeiss) digital camera. Confocal fluorescence microscopy was performed with an inverted microscope (Axiovert 200M; Carl Zeiss) equipped with Plan-Apochromat objectives, a spinning-disk head (Yokogawa) with emmision filters, and solid-state laser lines (488 and 561 nm). Confocal fluorescence and differential interference contrast (DIC) images were collected with a CoolSNAP-HQ2 digital camera (Roper Scientific) followed by processing with Metamorph imaging software (Universal Imaging). For actin staining with tetramethyl rhodamine isocyanate (TRITC)-conjugated phalloidin, cells were first washed with PBS, then fixed with 4% formaldehyde in PBS,

Downloaded from http://www.jbc.org/ at Shanghai Information Center for Life Sciences, Chinese Academy of Sciences on May 25, 2015

washed again, and permeabilized with 0.15% Triton X-100 in PBS. Following washing of the permeabilized cells with PBS, actin was stained for 1h at RT with TRITC-conjugated phalloidin (diluted 1:200 from a 50 µg/ml stock solution, Invitrogen). Subsequently, cells were washed with PBS, incubated for 10 min with 0.05% Tween-20 in PBS, washed successively with 70% EtOH and 100% EtOH, and finally embedded in Mowiol supplemented with DABCO (Sigma).

Preparation of whole-cell lysates and cell membrane fractions – Whole-cell lysates were prepared by washing cells directly in wells with ice-cold PBS, followed by lysis on ice in RIPA buffer (50 mM Tris-HCl/pH 7.5, 1% (wt/vol) Triton X-100, 1% (wt/vol) glycerol, 0.5% sodium deoxycholate, 0.1% sodium dodecylsulphate, 137 mM sodium chloride, 1 mM sodium orthovanadate, and 0.5 mM EDTA) complemented with Complete™ protease inhibitor cocktail. Cell debris was removed by centrifugation (21,000 g, 10 min, 4°C) and the protein concentration of the supernatant was measured with BCA protein assay kit (Uptima, Montluçon, France).

For the preparation of cell membrane fractions, cells were first washed in wells with ice-cold PBS and then scraped off into PBS including Complete™ protease inhibitor cocktail. Following sonication (3x30 sec, 80% power, 70% duty cycle) to disrupt the cell membrane, intact cells, nuclei and cell debris were removed by centrifugation (2,000 g, 5 min, 4°C) and supernatant centrifuged again (21,000 g, 2 h, 4°C) to obtain a pellet with the crude membrane fraction.

GST-based pull down assay – Glutathione Sepharose 4B beads were washed two times with GST-fish buffer (50 mM Tris/HCl pH7.5, 100 mM NaCl, 2 mM $MgCl_2$, 10% (w/v) glycerol, 1% (w/v) NP40), before incubation for 60 min at 4°C with 10 µg GST-RBD or the GST-RBD mutants and N- or C-terminal truncations, respectively. Beads were then washed two times with GST-fish buffer, incubated with GST-fish buffer containing 1% BSA, washed again with GST-fish buffer and incubated with 20 µg LSR_{Ig}-6His. Beads were then washed five times with GST-fish buffer. Bound proteins were eluted by addition of preheated (95 °C) Laemmli sample buffer and incubation for 10 min. Samples were then subjected to SDS-PAGE, followed by immunoblotting to detect the bait and prey proteins with specific antibodies.

Generation of a HCT116 cDNA library for the identification of LSR isoforms – Total RNA was isolated from HCT116 cells with the RNeasy Mini Kit (Qiagen) followed by cDNA synthesis with the First Strand cDNA Synthesis Kit (Thermo Scientific) using an oligo$(dT)_{18}$ primer according to the manufacturers´ instructions. LSR-specific cDNA transcripts were amplified by PCR using the forward primers 5´-GCAACAGGACGGACTTGGAGTAG-3´ (long N-terminus) or 5´-ATATCCATGGCGCTGTTGGCCGGCGG-3´ (short N-terminus) and the reverse primer 5´-TCAGACGACTAAACTTTCCCGACTCAGGGC C-3´. PCR products were finally cloned into the pCR-Blunt II-TOPO vector and analyzed by Sanger sequencing. Optionally, LSR isoforms were subcloned into the mammalian expression vectors ptdTomato-N1 or pEGFP-N1.

Statistics – Student´s t-test was used for pairwise comparison of the data and significance calculations.

RESULTS

CDT interacts with the extracellular, Ig-like domain of LSR–According to the protein database Uniprot, human LSR (accession number Q86X29) exists in 6 isoforms varying in length due to alternative splicing or differential translation initiation. Isoform 1 of LSR represents the canonical, non-spliced version of the protein with the length of 649 amino acids. The other isoforms are predicted to lack either small extracellular and/or intracellular protein segments, or even the putative transmembrane region and a cysteine-rich region.

In a previous study we cloned an LSR variant into a mammalian expression vector that derived from a human pancreatic adenocarcinoma cDNA library (20). Compared to isoform 1, this LSR variant (GenBank accession number AAH04381.2) lacks the first 48 amino acids of the N-terminus and a short segment (amino acids 240-258) between the Ig-like domain and the putative transmembrane region (Fig. 1A and 1B). However, as known from our previous study, the N-terminally shortened LSR variant efficiently promotes cell entry of CDT. Unless otherwise stated, this LSR variant is also used in the current study for functional analyses.

Intriguingly, isoform 6 of human LSR (UniProt accession number Q86X29-6), as well as all isoforms of murine LSR (Uniprot accession number

Downloaded from http://www.jbc.org/ at Shanghai Information Center for Life Sciences, Chinese Academy of Sciences on May 25, 2015

Q99KG5), also lack the N-terminal extension upstream of the Ig-like domain, which is present in human LSR (Fig. 1B).

We therefore wanted to test whether murine LSR can promote cell entry of CDT into HeLa cells that do not express detectable amounts of LSR and are highly resistant to the toxin. To this end, murine LSR (mLSR) was ectopically expressed in HeLa cells that were co-transfected with an EGFP-expressing plasmid to visualize the transfected cells. In addition, we also ectopically expressed the murine orthologs of ILDR1 (mILDR1) and ILDR2 (mILDR2), two members of the angulin family of tricellular tight junctions (tTJ)-associated proteins with homology to LSR (32) in the Ig-like domain. Addition of CDT caused cell rounding due to the destruction of the actin cytoskeleton only in mLSR-expressing HeLa cells, but not in cells that either expressed mILDR1 or mILDR2, or that expressed EGFP only (Fig. 1C). In addition, a FACS-based analysis of the binding of fluorescence-labeled CDTb to the cell surface of HeLa cells was performed. As expected, upon addition of labeled CDTb to HeLa cell suspensions, a strong increase in cell surface-bound fluorescence over background was only observed in a fraction of HeLa cells that expressed the mLSR protein (Fig. 1D). These results confirmed that the N-terminal extension found upstream of the Ig-like domain in human LSR isoforms is dispensable for binding and uptake of CDT and that the LSR-related proteins ILDR1 and ILDR2 do not serve as cell entry receptors for the toxin.

Therefore, we aimed to investigate whether CDT interacts with the Ig-like domain of LSR. To this end, we recombinantly expressed a DNA fragment encoding the Ig-like domain of human LSR as a C-terminally His-tagged protein (denoted as LSR_{Ig}-His6) with the pET expression system in *Escherichia coli*. The protein was mainly found in the pellet fraction after cell lysis and could be purified from inclusion bodies by urea-induced denaturation, followed by dialysis to remove the denaturation component for the refolding of the protein (Fig. 2A and 2B). We then used LSR_{Ig}-His6 as prey protein in a GST-pull down assay and a GST fusion of the receptor-binding domain (RBD) from CDTb (amino acids 677 to 876) as bait. LSR-dependent cell surface-binding of GST-RBD was shown previously (31). As shown in Fig. 2C, the LSR_{Ig}-His6 protein co-precipitated with GST-RBD-loaded glutathione beads but not with beads that were loaded with GST only. To confirm the direct interaction between the immunoglobulin-like domain of LSR and the receptor-binding domain of CDTb, we performed surface plasmon resonance (SPR) spectroscopy measurements. The LSR_{Ig}-His6 protein was immobilized on a sensor chip and the binding kinetics of GST or GST-RBD were measured. A biphasic association and dissociation profile was only obvious for GST-RBD but not for the GST protein (Fig. 2D). Thereby, we obtained a dissociation constant (K_D) of ~110 nM for the interaction between GST-RBD and LSR_{Ig}-His6.

Next, we wanted to determine the binding kinetics of the receptor-binding domain of CDTb when it binds to LSR in its native environment in the plasma membrane. For this purpose, we chose H1-HeLa(+LSR) cells that ectopically express the LSR variant AAH04381.2 and two human colon carcinoma-derived cell lines (CaCo-2, HCT116), because CDT is a toxin from an intestinal pathogen. Cell suspensions were incubated with increasing concentrations of fluorescence-labeled GST-RBD at 4°C to prevent endocytic uptake, followed by FACS analysis to measure the cell surface-bound fluorescence of the cells. GST-RBD revealed saturable binding to all three cell lines (Fig. 3), thereby allowing the calculation of the following K_D values: 40.4±9.3 nM for H1-HeLa(+LSR), 42.6±13.9 nM for CaCo-2, and 32.6±4.7 nM for HCT116 cells. As a comparison, for the binding of CDTb to HCT116 cells, we obtained by the same approach a K_D value of 47.6±2.8 nM. These K_D values for the interaction of GST-RBD with LSR at the cell surface were in good agreement with the binding constant that was obtained by SPR measurements for the interaction between GST-RBD and the immunoglobulin-like domain of LSR.

Generation and evaluation of an HCT116 LSR knockout cell line for functional studies–We next decided to generate a defined LSR knockout cell line in order to be able to ectopically express various LSR mutants for functional studies. We chose the human, colon carcinoma-derived cell line HCT116 for this purpose and applied the CRISPR-Cas9 technology to disrupt the LSR gene. Hence, we were able to isolate an HCT116 clone with a base pair insertion between positions 518/519 of the LSR coding region (termed $HCT116_{\Delta LSR}$ in this study), which leads to a frame shift mutation in exon 2 and to incomplete translation of the LSR protein (Fig. 4A). Immunoblot analysis with an LSR-specific antibody confirmed that LSR is not

Downloaded from http://www.jbc.org/ at Shanghai Information Center for Life Sciences, Chinese Academy of Sciences on May 25, 2015

expressed in HCT116$_{\Delta LSR}$ cells (Fig. 4B). We then transduced the HCT116$_{\Delta LSR}$ cells with a FLAG- or FLAG-LSR-encoding retrovirus for functional reconstitution studies. The ectopic expression of FLAG-LSR could be confirmed in FLAG-LSR-tranduced HCT116$_{\Delta LSR}$ cells by an anti-LSR immunoblot analysis of the membrane fraction (Fig. 4C). HCT116 wild-type and LSR knockout cells, as well as FLAG- and FLAG-LSR-transduced HCT116$_{\Delta LSR}$ cells, were incubated with CDT for 24 h, followed by microscopic analysis of the cell morphology. As expected, HCT116$_{\Delta LSR}$ and FLAG-transduced HCT116$_{\Delta LSR}$ cells remained fully resistant towards CDT and toxin-induced cell rounding was obvious only in wild-type HCT116 cells and FLAG-LSR-expressing HCT116$_{\Delta LSR}$ cells (Fig. 4D). FACS analysis with DyLight488-labeled GST-RBD additionally proved the cell surface expression of LSR only in wild-type HCT116 cells and FLAG-LSR-expressing HCT116$_{\Delta LSR}$ cells, but not in non- or FLAG-only-transduced HCT116$_{\Delta LSR}$ cells (Fig. 4E). These results confirmed that the HCT116$_{\Delta LSR}$ cells are suitable for the task to express different LSR mutants or isoforms for functional studies.

Identification of multiple isoforms of LSR in HCT116 cells–We were also interested in the identification of LSR isoforms that are expressed in HCT116 cells. To this end we isolated the total RNA of HCT116 cells for cDNA synthesis using an oligo(dT)$_{18}$ primer. The cDNA mixture was then used to amplify possible LSR isoforms via PCR with LSR-specific oligonucleotides. PCR products were finally cloned into the pCR-Blunt II-TOPO vector and analyzed by Sanger sequencing. Surprisingly, we never obtained any PCR product when the LSR reverse primer was used in combination with an LSR forward primer that was complementary to the starting sequence of the canonical LSR isoform (isoform 1). However, PCR products were obtained when the LSR reverse primer was combined with an LSR forward primer that was complementary to the starting sequence of the shortened LSR isoforms (e.g., LSR isoform 6 and LSR variant AAH04381.2). We found at least 4 different isoforms in HCT116 cells, all with potentially shortened N-terminus. Three isoforms represent the same splice variants as LSR isoforms 3, 5, and 6 (UniProt accession numbers: Q86X29-3, Q86X29-5. Q86X29-6). Interestingly, we found a previously unknown splice variant in HCT116 cells that is not annotated in the UniProt database. This LSR splice variant is lacking a large central part of the protein. We designate this novel LSR splice variant as LSR isoform 7. The LSR isoforms that we identified in HCT116 cells are schematically represented in Figure 5A, in direct comparison to already known LSR isoforms from the UniProt database. It is also of note that we found single amino acid deletions or insertions in the cytoplasmic tail of the LSR isoforms from HCT116 cells that differ from the canonical sequence (Figure 5A; indicated with Greek symbols).

Obviously, some LSR isoforms found in HCT116 cells lack the putative transmembrane helix (TH) and the cysteine-rich region (CR) in the central part of the protein and we wanted to clarify whether this part of LSR is required for integration of the protein into the plasma membrane. To this end, isoform-3-like (with TH/CR) and isoform-5-like (w/o TH/CR) LSR proteins were co-expressed ectopically in HCT116$_{\Delta LSR}$ cells as C-terminally Tomato- and EGFP-fused proteins, respectively, prior to confocal fluorescence microscopy. Isoform-3-like LSR clearly localized to the cell periphery of HCT116$_{\Delta LSR}$ cells, whereas, in contrast, isoform-5-like LSR exhibited an intracellular staining pattern (Fig. 5B). Interestingly, isoform-5-like LSR clearly colocalized with a co-expressed endoplasmic reticulum (ER) marker protein (cal-dsRed2) (Fig. 5C). These observations point out to the fact that the putative transmembrane helix and cysteine-rich region are required for targeting and insertion of LSR into the plasma membrane. LSR isoforms lacking the transmembrane helix and cysteine-rich region most likely represent ER-resident proteins.

The cytoplasmic tail and the cysteine-rich region of LSR are not essential for targeting of the receptor to the plasma membrane and for cell entry of CDT–We next took again advantage of the HCT116$_{\Delta LSR}$ cells to transiently express EGFP or Tomato fusion proteins of full-length LSR (LSR-EGFP/Tomato) and LSR truncations that either lacked the cytoplasmic tail (LSR$_{1-240}$-EGFP/Tomato) or the cysteine-rich region (LSR$_{\Delta CR}$-EGFP/Tomato) (Fig. 6A). Following the transfection of the LSR knockout cells with the respective plasmids, we first aimed to validate whether the LSR truncations are expressed and properly targeted to the plasma membrane. As shown in Fig. 6B, one day after transfection, expression of LSR-EGFP, LSR$_{1-240}$-EGFP and LSR$_{\Delta CR}$-EGFP could be confirmed in HCT116$_{\Delta LSR}$

Downloaded from http://www.jbc.org/ at Shanghai Information Center for Life Sciences, Chinese Academy of Sciences on May 25, 2015

cells by performing an anti-EGFP immunoblot analysis with the solubilized membrane fractions. As expected, no protein could be detected by the anti-EGFP antibody in membrane fractions of non-transfected HCT116 and HCT116$_{\Delta LSR}$ cells. Transient expression of LSR-EGFP and LSR$_{\Delta CR}$-EGFP in HCT116$_{\Delta LSR}$ cells, as well as native expression of LSR in wild-type HCT116 cells, could be further confirmed with an anti-LSR antibody that recognizes a region at the C-terminal end of LSR. The anti-LSR antibody did not recognize LSR$_{1-240}$-EGFP, because the antibody recognizes an epitope at the C-terminal end of LSR which is missing in this truncated version of LSR (Fig. 6B).

To further validate that the LSR truncations are properly targeted to the plasma membrane with extracellular exposure of the Ig-like domain, a FACS-based analysis of the binding of fluorescence-labeled GST-RBD to the cell surface was performed. For this purpose, the HCT116$_{\Delta LSR}$ cells were transiently transfected with plasmids encoding the Tomato fusion proteins of LSR and its truncated variants, prior to incubation of the cells with green fluorescence-labeled GST-RBD. Following a gating procedure to discriminate between the non-transfected (region 1; R1) and the transfected cell fraction expressing the Tomato constructs (region 2; R2), binding of green fluorescence-labeled GST-RBD to the cell surface of the R1 or the R2 fraction was analyzed in two-dimensional dot plots (green fluorescence versus side scatter). As expected, the non-transfected fraction of HCT116$_{\Delta LSR}$ cells (R1) did not show any binding of green-labeled GST-RBD. However, an increase of cell surface-bound green fluorescence was observed in the R2 fractions, representing the LSR-Tomato-, LSR$_{1-240}$-Tomato- and LSR$_{\Delta CR}$-Tomato-expressing HCT116$_{\Delta LSR}$ cells (Fig. 6C). These results indicated that full-length and both truncated LSR variants were properly targeted to the plasma membrane and that the Ig-like domain of LSR variants is correctly folded and exposed at the cell surface to allow the binding of the receptor-binding domain of CDTb. The data allow the conclusion that the cysteine-rich region and the cytoplasmic tail of LSR are not required for plasma membrane integration of the receptor.

We then wanted to analyze whether the cytoplasmic tail or the cysteine-rich region of LSR is essential for endocytic uptake of CDT. For that purpose, HCT116$_{\Delta LSR}$ cells were transfected with plasmids for the expression of LSR-EGFP, LSR$_{1-240}$-EGFP or LSR$_{\Delta CR}$-EGFP followed by incubation with CDT for 3 h at 37°C. TRITC-phalloidin staining and confocal fluorescence microscopy was then applied to visualize the toxin-induced disruption of the actin cytoskeleton. As shown in Fig. 7, LSR-EGFP-expressing cells were susceptible to CDT, since the actin cytoskeleton in these cells could not be stained with TRITC-phalloidin after incubation with the toxin. Moreover, toxin-induced cell rounding was clearly recognizable only in LSR-EGFP-expressing cells (Fig. 7, DIC image). As expected, non-transfected HCT116$_{\Delta LSR}$ cells (cells without green fluorescence) remained resistant to the toxin (Fig. 7). However, CDT-induced depolymerization of the actin cytoskeleton was also observed in LSR$_{1-240}$-EGFP- and LSR$_{\Delta CR}$-EGFP-expressing cells, indicating that also in these cells CDT was endocytosed and active (Fig. 7).

Taken together, our findings indicate that binding and uptake of CDT does not essentially require the cytoplasmic tail or the cysteine-rich region of LSR.

Amino acids 757 to 866 of CDTb are sufficient for the interaction with the Ig-like domain of LSR– Marvaud and colleagues mapped the receptor-binding domain of the iota toxin to the C-terminus of its binding component (Ib) (35). CDT is a member of the iota-like toxin family and we recently confirmed this finding with a GST fusion of the C-terminus of CDTb (GST-RBD) that bound directly to LSR-expressing cells and competitively inhibited the binding of CDTb to the cell surface (31).

Our next aim was to narrow down the region within the receptor-binding domain (RBD; amino acids 677 to 876) of CDTb that is sufficient for the interaction with the Ig-like domain of LSR. Accordingly, we generated a series of GST fusion proteins with N- or C-terminal truncations of RBD (Fig. 8A) and tested whether LSR$_{Ig}$-His6 co-precipitates with the GST fusion proteins in a pull down approach. As shown in Fig. 8B, deletion of the N-terminal 80 amino acids (RBD/Δ80N; GST-RBD$_{aa757-876}$) or the C-terminal 10 amino acids of RBD (RBD/Δ10C; GST-RBD$_{aa677-866}$) did not abolish the binding of LSR$_{Ig}$-His6 (Fig. 8B, upper panel). However, LSR$_{Ig}$-His6 did not bind to RBD truncations that lacked 120 N-terminal (RBD/Δ120N; GST-RBD$_{aa797-876}$) or 20 C-terminal

Downloaded from http://www.jbc.org/ at Shanghai Information Center for Life Sciences, Chinese Academy of Sciences on May 25, 2015

amino acids (RBD/Δ20C; GST-RBD$_{aa677-856}$), respectively (Fig. 8B, lower panel).

To substantiate these findings, we performed FACS competition experiments, where fluorescence-labeled GST-RBD (RBD$_{DL488}$) was incubated with H1-HeLa(+LSR) cell suspensions either alone or together with 1-, 10- or 100-fold molar excess of non-labeled N- or C-terminal truncations of RBD. Concomitantly, FACS analyses revealed that RBD/Δ80N and RBD/Δ10C (Fig. 8C and 8D, white bars), but not RBD/Δ120N and RBD/Δ20C (Fig. 8C and 8D, black bars), competitively inhibited the binding of fluorescence-labeled RBD to H1-HeLa(+LSR) cells. Notably, a 100-fold excess of RBD/Δ10C was necessary to strongly decrease the binding of RBD$_{DL488}$, indicating that the C-terminal 10 amino acids of RBD might enhance the interaction with the toxin but are not essential. From these results it can be concluded that a relatively small region between amino acids 757 to 866 of CDTb is already sufficient for the interaction with LSR. It seems that CDTb$_{757-866}$ represents the precise receptor-binding domain of the toxin.

To identify epitopes within the receptor-binding domain of CDTb that are crucial for the interaction with LSR, we carried out a transposon-based mutagenesis approach with a plasmid encoding GST-RBD. We obtained 8 independent GST-RBD mutants (T1-T8), each containing a 5-amino acid in-frame insertion at different positions within the amino acid range 757 to 876 of the RBD (Fig. 9A and 9B). To test whether the 5-amino acid linker disturbs an important epitope required for the interaction with LSR, we again performed a FACS competition experiment as described above. Now, fluorescence-labeled GST-RBD (RBD$_{DL488}$) was incubated with H1-HeLa(+LSR) cell suspensions either alone or together with 1-, 10- or 100-fold molar excess of non-labeled GST-RBD (RBD) or the non-labeled GST-RBD mutants (T1-T8). Then the amount of cell surface bound fluorescence was analyzed by FACS analysis.

As shown in Fig. 9C, non-labeled GST-RBD (RBD), as well as the GST-RBD mutants T1, T3, T6, and T7, notably inhibited the binding of RBD$_{DL488}$ to H1-HeLa(+LSR) cells already at a molar ratio of 1:1 (RBD$_{DL488}$: competing protein). Clear inhibition of RBD$_{DL488}$ binding to H1-HeLa(+LSR) cells was observed for the T4, T5 and T8 mutants only when the proteins were conincubated in a 10-fold molar excess together with RBD$_{DL488}$. Interestingly, the GST-RBD mutant T2 decreased binding of RBD$_{DL488}$ only when coincubated in a 100-fold excess together with RBD$_{DL488}$. To validate the correct folding of the GST-RBD mutant T2, we performed limited proteolysis of RBD and T2 by incubating the proteins with increasing concentrations of trypsin for 10 min at 4°C. As shown in Fig. 9D, RBD and T2 exhibited a similar pattern of proteolytical fragments after incubation with increasing concentrations of trypsin, indicating that the 5-amino acid insertion in the T2 mutant did not alter the overall structure of the protein. Taken together, the FACS competition analyses indicated that the 5-amino acid linkers which are present in the GST-RBD mutants T4, T5, T8, and especially in the GST-RBD mutant T2, may disturb an important LSR-interacting epitope and, thereby, decrease the affinity of the RBD for binding to LSR.

DISCUSSION

LSR is a type-I transmembrane protein exposing its N-terminal part at the cell surface. The extracellular part of LSR can be subdivided into two regions, an uncharacterized region at the N-terminus followed by an immunoglobulin (Ig)-like, V-type domain (36). Both regions could serve independently or together as a platform for the interaction with CDT. In reference to the UniProt protein entries for LSR, the N-terminus of the mouse LSR ortholog is much shorter (~33 amino acids) when compared to human LSR (~86 amino acids). However, human LSR variants exist that also feature a shortened N-terminus (e.g. LSR isoform 6). Furthermore, we previously studied the uptake of CDT into cultured cells with an LSR variant that was cloned from a human pancreatic adenocarcinoma cDNA library (20). This LSR variant exhibits a shortened N-terminus (~38 amino acids), identical to isoform 6 of human LSR and similar to the mouse LSR ortholog, and was fully functional in terms of mediating cellular uptake of the toxin. Consistently, as shown in the current study, ectopically expressed mouse LSR efficiently promoted cell entry of CDT in HeLa cells.

From these findings we hypothesized that CDT interacts most likely with the Ig-like domain of LSR. By performing co-precipitation analyses, we confirmed the direct binding of the receptor-binding domain (RBD) of CDTb to the Ig-like domain of LSR and obtained by SPR measurements a K_D value of ~110 nM for this interaction. Similar dissociation

Downloaded from http://www.jbc.org/ at Shanghai Information Center for Life Sciences, Chinese Academy of Sciences on May 25, 2015

constants were calculated for the binding of RBD to the surface of various cultured cells via FACS analysis (K_D: ~30 to ~40 nM). An Ig-like domain is also present in ANTXR1 (TEM8) and ANTXR2 (CMG2), two known receptors of anthrax toxin. In contrast to CDT, anthrax toxin does not interact with the Ig-like domain of its receptors but binds with a very high affinity (K_D: ~0.2 nM for CMG2) to a von Willenbrand factor A (VWA) domain that is located in front of the Ig-like domain within the extracellular domain (37-39). However, it has been shown that the Ig-like domain of CMG2 is essential for proper functioning of the receptor-bound PA pore (40). Furthermore, the crystal structure of the PA-CMG2 complex, as well as a study from Pilpa and colleagues, confirmed the involvement of the CMG2 receptor in PA pore formation (41,42). Thus, it remains to be studied whether the Ig-like domain of LSR participates in the pore formation of the B component of CDT.

The intracellular domain of LSR contains a cysteine-rich region directly after the transmembrane helix followed by a cytoplasmic tail. So far, no functional roles have been attributed to the cysteine-rich region or the cytoplasmic tail of LSR. LSR mutants that either lack the cysteine-rich region or the cytoplasmic tail were properly targeted to the plasma membrane of HCT116 LSR knockout cells. To our surprise, intoxication of HCT116 LSR knockout cells with CDT still occurred with both mutants. These results raise the important question of how the endocytic uptake of LSR is triggered since the cysteine-rich region and the cytoplasmic tail are not required for the uptake of CDT. It is conceivable that the endocytosis of LSR is triggered also by other membrane proteins, which might form a complex with LSR. We found recently that LSR accumulates in lipid rafts upon binding of CDTb (31). Interestingly, Wigelsworth and colleagues found that the lipid rafts-associated protein CD44 is crucial for CDT uptake into host cells (43). CD44 is therefore a suitable candidate that could bind to LSR and trigger the endocytic uptake of the protein complex. However, a physical interaction between LSR and CD44 has not been described until now. It remains to be addressed in the future, whether the cysteine-rich region or the cytoplasmic tail of LSR contributes to other physiological functions of LSR besides uptake of CDT.

All isoforms of LSR can be subdivided into two groups, depending on the presence or absence of the transmembrane segment plus the cysteine-rich region in the central part of the receptor. As we show in this study, the absence of the transmembrane segment and cysteine-rich region of LSR renders the protein unable to integrate into the plasma membrane and such isoforms are most likely retained in the ER with unknown physiological consequences. It might also be possible that LSR variants that are not capable of integrating into the plasma membrane represent partially secreted proteins. One can speculate that secreted LSR variants might block LSR-dependent intracellular signaling pathways by acting as decoy receptors for extracellular ligands. Secreted LSR variants could also serve as ligands for other cell surface receptors. Since LSR is involved in the formation of tricellular tight junctions, it would be of particular interest to analyze whether the expression levels of different LSR isoforms differ between confluent and non-confluent cultured cells.

Another aim of this study was to narrow down the region and to identify possible epitopes within the receptor-binding domain of CDTb that are essential for interaction with LSR. Based on truncated variants of the B component of iota-toxin (Ib), Marvaud and colleagues confirmed the presence of the receptor-binding domain (RBD) at the C-terminal part of Ib (35). The RBD of Ib corresponds to amino acids 677 to 876 of CDTb and we recently confirmed that this region of CDTb binds to LSR exposed at the cell surface (31). The current study suggests that amino acids 757 to 866 of CDTb are sufficient for the interaction with LSR. In a previous study, a truncated Ib variant lacking only the C-terminal 10 residues was not able to bind to Vero cells, which is in contrast to our results that we obtained with a CDTb RBD mutant lacking also 10 C-terminal amino acids (35).The authors of this study used Ib truncations with a cleaved His-tag in their experiments rather than GST-fused constructs as we did for our CDTb truncations. However, we also noticed a decreased binding of the RBD truncation lacking the 10 C-terminal amino acids to the Ig-like domain of LSR. The C-terminal end of the B components of iota-like toxins might be important for the conformational integrity of the proteins.

Our transposon-based mutagenesis approach to identify important epitopes in the RBD of CDTb that are crucial for the interaction with LSR yielded four mutants with decreased ability to compete the cell surface-binding of the RBD. Interestingly, the

Downloaded from http://www.jbc.org/ at Shanghai Information Center for Life Sciences, Chinese Academy of Sciences on May 25, 2015

T2 mutant which showed the weakest competitive potential, contained a 5-amino acid in-frame insertion between amino acids 853 and 854. Strikingly, this position lies in between the amino acids 843 to 866 of CDTb, a region corresponding to a linear epitope in Ib, which is recognized by a monoclonal antibody that inhibits *in vitro* cytotoxicity of iota-toxin (35,44). The 5-amino acid insertions of the T4 and T8 mutants were also found within the neutralizing epitope, confirming that this region most likely interacts with the LSR protein. However, the T5 mutant contained a 5-amino acid insertion in between amino acids 781 and 782, indicating an additional epitope in the RBD of CDTb which might be important for the interaction with LSR.

Taken together, our findings provide novel insights into the interaction between CDT and its receptor LSR. A precise knowledge about specific binding regions enables the development of anti-toxin strategies that might help to prevent cell entry of the toxin and, potentially, to prevent the outcome of the toxin-associated disease symptoms.

REFERENCES

1. Rupnik, M., Wilcox, M. H., and Gerding, D. N. (2009) *Clostridium difficile* infection: new developments in epidemiology and pathogenesis. *Nat. Rev. Microbiol.* **7,** 526-536
2. Voth, D. E. and Ballard, J. D. (2005) *Clostridium difficile* toxins: mechanism of action and role in disease. *Clin. Microbiol. Rev.* **18,** 247-263
3. Kelly, C. P. and LaMont, J. T. (1998) *Clostridium difficile* infection. *Annu. Rev. Med.* **49,** 375-390
4. McDonald, L. C., Killgore, G. E., Thompson, A., Owens, R. C., Jr., Kazakova, S. V., Sambol, S. P., Johnson, S., and Gerding, D. N. (2005) An epidemic, toxin gene-variant strain of *Clostridium difficile*. *N. Engl. J. Med.* **353,** 2433-2441
5. Kelly, C. P. and LaMont, J. T. (2008) *Clostridium difficile*--more difficult than ever. *N. Engl. J. Med.* **359,** 1932-1940
6. O'Connor, J. R., Johnson, S., and Gerding, D. N. (2009) *Clostridium difficile* infection caused by the epidemic BI/NAP1/027 strain. *Gastroenterology* **136,** 1913-1924
7. Kyne, L. (2010) *Clostridium difficile*--beyond antibiotics. *N. Engl. J. Med.* **362,** 264-265
8. Perelle, S., Gibert, M., Bourlioux, P., Corthier, G., and Popoff, M. R. (1997) Production of a complete binary toxin (actin-specific ADP-ribosyltransferase) by *Clostridium difficile* CD196. *Infect. Immun.* **65,** 1402-1407
9. Gerding, D. N., Johnson, S., Rupnik, M., and Aktories, K. (2014) *Clostridium difficile* binary toxin CDT: Mechanism, epidemiology, and potential clinical importance. *Gut Microbes* **5,** 15-27
10. Stiles, B. G., Pradhan, K., Fleming, J. M., Samy, R. P., Barth, H., and Popoff, M. R. (2014) *Clostridium* and *bacillus* binary enterotoxins: bad for the bowels, and eukaryotic being. *Toxins (Basel)* **6,** 2626-2656
11. Barth, H., Blöcker, D., Behlke, J., Bergsma-Schutter, W., Brisson, A., Benz, R., and Aktories, K. (2000) Cellular uptake of *Clostridium botulinum* C2 toxin requires oligomerization and acidification. *J. Biol. Chem.* **275,** 18704-18711
12. Barth, H. (2004) Uptake of binary actin ADP-ribosylating toxins. *Rev. Physiol. Biochem. Pharmacol.* **152,** 165-182
13. Aktories, K. and Barth, H. (2004) *Clostridium botulinum* C2 toxin--new insights into the cellular up-take of the actin-ADP-ribosylating toxin. *Int. J. Med. Microbiol.* **293,** 557-564
14. Young, J. A. and Collier, R. J. (2007) Anthrax toxin: receptor-binding, internalization, pore formation, and translocation. *Annu. Rev. Biochem.* **76,** 243-265
15. Aktories, K., Bärmann, M., Ohishi, I., Tsuyama, S., Jakobs, K. H., and Habermann, E. (1986) Botulinum C2 toxin ADP-ribosylates actin. *Nature* **322,** 390-392
16. Barth, H., Aktories, K., Popoff, M. R., and Stiles, B. G. (2004) Binary bacterial toxins: biochemistry, biology, and applications of common *Clostridium* and *Bacillus* proteins. *Microbiol. Mol. Biol. Rev.* **68,** 373-402
17. Stiles, B. G., Wigelsworth, D. J., Popoff, M. R., and Barth, H. (2011) Clostridial binary toxins: iota and c2 family portraits. *Front. Cell. Infect. Microbiol.* **1,** 11

Downloaded from http://www.jbc.org/ at Shanghai Information Center for Life Sciences, Chinese Academy of Sciences on May 25, 2015

18. Kaiser, E., Kroll, C., Ernst, K., Schwan, C., Popoff, M., Fischer, G., Buchner, J., Aktories, K., and Barth, H. (2011) Membrane translocation of binary actin-ADP-ribosylating toxins from *Clostridium difficile* and *Clostridium perfringens* is facilitated by Cyclophilin A and Hsp90. *Infect. Immun.* **79,** 3913-3921
19. Schwan, C., Stecher, B., Tzivelekidis, T., van, H. M., Rohde, M., Hardt, W. D., Wehland, J., and Aktories, K. (2009) *Clostridium difficile* toxin CDT induces formation of microtubule-based protrusions and increases adherence of bacteria. *PLoS Pathog* **5,** e1000626
20. Papatheodorou, P., Carette, J. E., Bell, G. W., Schwan, C., Guttenberg, G., Brummelkamp, T. R., and Aktories, K. (2011) Lipolysis-stimulated lipoprotein receptor (LSR) is the host receptor for the binary toxin *Clostridium difficile* transferase (CDT). *Proc. Natl. Acad. Sci. U. S. A* **108,** 16422-16427
21. Papatheodorou, P., Wilczek, C., Nolke, T., Guttenberg, G., Hornuss, D., Schwan, C., and Aktories, K. (2012) Identification of the cellular receptor of *Clostridium spiroforme* toxin. *Infect. Immun.* **80,** 1418-1423
22. Schmidt, G., Papatheodorou, P., and Aktories, K. (2014) Novel receptors for bacterial protein toxins. *Curr. Opin. Microbiol.* **23,** 55-61
23. Yen, F. T., Mann, C. J., Guermani, L. M., Hannouche, N. F., Hubert, N., Hornick, C. A., Bordeau, V. N., Agnani, G., and Bihain, B. E. (1994) Identification of a lipolysis-stimulated receptor that is distinct from the LDL receptor and the LDL receptor-related protein. *Biochemistry* **33,** 1172-1180
24. Yen, F. T., Masson, M., Clossais-Besnard, N., Andre, P., Grosset, J. M., Bougueleret, L., Dumas, J. B., Guerassimenko, O., and Bihain, B. E. (1999) Molecular cloning of a lipolysis-stimulated remnant receptor expressed in the liver. *J. Biol. Chem.* **274,** 13390-13398
25. Mesli, S., Javorschi, S., Berard, A. M., Landry, M., Priddle, H., Kivlichan, D., Smith, A. J., Yen, F. T., Bihain, B. E., and Darmon, M. (2004) Distribution of the lipolysis stimulated receptor in adult and embryonic murine tissues and lethality of LSR-/- embryos at 12.5 to 14.5 days of gestation. *Eur. J. Biochem.* **271,** 3103-3114
26. Bihain, B. E. and Yen, F. T. (1998) The lipolysis stimulated receptor: a gene at last. *Curr. Opin. Lipidol.* **9,** 221-224
27. Yen, F. T., Roitel, O., Bonnard, L., Notet, V., Pratte, D., Stenger, C., Magueur, E., and Bihain, B. E. (2008) Lipolysis stimulated lipoprotein receptor: a novel molecular link between hyperlipidemia, weight gain, and atherosclerosis in mice. *J. Biol. Chem.* **283,** 25650-25659
28. Furuse, M., Oda, Y., Higashi, T., Iwamoto, N., and Masuda, S. (2012) Lipolysis-stimulated lipoprotein receptor: a novel membrane protein of tricellular tight junctions. *Ann. N. Y. Acad. Sci.* **1257,** 54-58
29. Masuda, S., Oda, Y., Sasaki, H., Ikenouchi, J., Higashi, T., Akashi, M., Nishi, E., and Furuse, M. (2011) LSR defines cell corners for tricellular tight junction formation in epithelial cells. *J. Cell Sci.* **124,** 548-555
30. Mali, P., Yang, L., Esvelt, K. M., Aach, J., Guell, M., DiCarlo, J. E., Norville, J. E., and Church, G. M. (2013) RNA-guided human genome engineering via Cas9. *Science* **339,** 823-826
31. Papatheodorou, P., Hornuss, D., Nolke, T., Hemmasi, S., Castonguay, J., Picchianti, M., and Aktories, K. (2013) *Clostridium difficile* binary toxin CDT induces clustering of the lipolysis-stimulated lipoprotein receptor into lipid rafts. *MBio* **4,** e00244-13
32. Higashi, T., Tokuda, S., Kitajiri, S. I., Masuda, S., Nakamura, H., Oda, Y., and Furuse, M. (2012) Analysis of the angulin family consisting of LSR, ILDR1 and ILDR2: tricellulin recruitment, epithelial barrier function and implication in deafness pathogenesis. *J. Cell Sci.* **126**, 966-977
33. Schwan, C., Noelke, T., Kruppke, A. S., Schubert, D. M., Lang, A. E., and Aktories, K. (2011) Cholesterol- and sphingolipid-rich microdomains are essential for microtubule-based membrane protrusions induced by *Clostridium difficile* transferase CDT. *J. Biol. Chem.* **286,** 29356-29365
34. Sterthoff, C., Lang, A. E., Schwan, C., Tauch, A., and Aktories, K. (2010) Functional characterization of an extended binding component of the actin-ADP-ribosylating C2 toxin detected in *Clostridium botulinum* strain (C) 2300. *Infect. Immun.* **78,** 1468-1474

Downloaded from http://www.jbc.org/ at Shanghai Information Center for Life Sciences, Chinese Academy of Sciences on May 25, 2015

35. Marvaud, J. C., Smith, T., Hale, M. L., Popoff, M. R., Smith, L. A., and Stiles, B. G. (2001) *Clostridium perfringens* iota-toxin: mapping of receptor binding and Ia docking domains on Ib. *Infect. Immun.* **69,** 2435-2441
36. Furuse, M., Izumi, Y., Oda, Y., Higashi, T., and Iwamoto, N. (2014) Molecular organization of tricellular tight junctions. *Tissue Barriers* **2,** e28960
37. Bradley, K. A., Mogridge, J., Mourez, M., Collier, R. J., and Young, J. A. (2001) Identification of the cellular receptor for anthrax toxin. *Nature* **414,** 225-229
38. Scobie, H. M., Rainey, G. J., Bradley, K. A., and Young, J. A. (2003) Human capillary morphogenesis protein 2 functions as an anthrax toxin receptor. *Proc. Natl. Acad. Sci. U. S. A* **100,** 5170-5174
39. Wigelsworth, D. J., Krantz, B. A., Christensen, K. A., Lacy, D. B., Juris, S. J., and Collier, R. J. (2004) Binding stoichiometry and kinetics of the interaction of a human anthrax toxin receptor, CMG2, with protective antigen. *J. Biol. Chem.* **279,** 23349-23356
40. Sun, J. and Collier, R. J. (2010) Disulfide bonds in the ectodomain of anthrax toxin receptor 2 are required for the receptor-bound protective-antigen pore to function. *PLoS One* **5,** e10553
41. Santelli, E., Bankston, L. A., Leppla, S. H., and Liddington, R. C. (2004) Crystal structure of a complex between anthrax toxin and its host cell receptor. *Nature* **430,** 905-908
42. Pilpa, R. M., Bayrhuber, M., Marlett, J. M., Riek, R., and Young, J. A. (2011) A receptor-based switch that regulates anthrax toxin pore formation. *PLoS Pathog* **7,** e1002354
43. Wigelsworth, D. J., Ruthel, G., Schnell, L., Herrlich, P., Blonder, J., Veenstra, T. D., Carman, R. J., Wilkins, T. D., Van Nhieu, G. T., Pauillac, S., Gibert, M., Sauvonnet, N., Stiles, B. G., Popoff, M. R., and Barth, H. (2012) CD44 promotes intoxication by the clostridial iota-family toxins. *PLoS One* **7,** e51356
44. Stiles, B. G., Hale, M. L., Marvaud, J. C., and Popoff, M. R. (2002) *Clostridium perfringens* iota toxin: characterization of the cell-associated iota b complex. *Biochem. J.* **367,** 801-808

Acknowledgments–We thank Otilia Wunderlich for excellent technical assistance, Carsten Schwan for help in microscopy, Thijn Brummelkamp (Netherlands Cancer Institute, Amsterdam, The Netherlands) for valuable advice concerning CRISPR-Cas9 technology, Maximilian Mauler for assistance in FACS measurements, and Mikio Furuse (Kobe University, Japan) for sharing plasmids.

FOOTNOTES

*This work was supported by the Deutsche Forschungsgemeinschaft (AK6/20-1) and the Centre for Biological Signaling Studies (BIOSS) in Freiburg, Germany

[6]The abbreviations used are: CDT, *Clostridium difficile* transferase; LSR, lipolysis-stimulated lipoprotein receptor; RBD, receptor-binding domain; gRNA, guide RNA; CRISPR, clustered regularly interspaced short palindromic repeats; PAM, protospacer adjacent motif; RU, response units; ATP1A1, sodium/potassium-transporting ATPase subunit alpha-1; BCA, bicinchoninic acid assay; ILDR1/2, immunoglobulin-like domain containing receptor 1/2; Ig, immunoglobulin; TH, transmembrane helix; CR, cysteine-rich region; ER, endoplasmic reticulum; DIC, differential interference contrast; GST, glutathione S-transferase; NHS, N-hydroxysulfosuccinimide; ANTXR1/2, anthrax toxin recptor 1/2; TEM8, tumor endothelial marker 8; CMG2, capillary morphogenesis gene 2 protein; PA, protective antigen; CD44, cluster of differentiation 44 protein

[$]These authors contributed equally to this work

FIGURE LEGENDS

FIGURE 1. The mouse ortholog of human LSR exhibits a shortened N-terminus and is sufficient for binding and cellular uptake of CDT. (A) Schematic representation of the domain architecture of the isoform 1 of human LSR ($hLSR_{Q86X29\text{-}1}$) in comparison to a human LSR variant cloned from a human pancreatic adenocarcinoma cDNA library ($hLSR_{AAH04381.2}$). TH, transmembrane helix; CR, cysteine-rich region. (B) Multiple sequence alignment of the N-terminal part of the human LSR (hLSR) versions Q86X29-1 and

Downloaded from http://www.jbc.org/ at Shanghai Information Center for Life Sciences, Chinese Academy of Sciences on May 25, 2015

AAH04381.2 and the human LSR mouse ortholog (mLSR) Q99KG5. Asterisk, identical amino acids; Dot and double dot, similar amino acids. (C) CDT intoxication of HeLa cells ectopically expressing mLSR, mILDR1, and mILDR2. HeLa cells were co-transfected with an EGFP-expressing plasmid together with an empty vector (EV) or together with plasmids encoding either murine LSR (mLSR) or the two LSR-homologous murine proteins ILDR1 (mILDR1) and ILDR2 (mILDR2). One day after transfection, cells were incubated with CDT overnight at 37°C, prior to the analysis of the cell morphology of the co-transfected cells via fluorescence microscopy. (D) FACS-based analysis of the binding of DyLight488-labeled CDTb to the cell surface of transfected HeLa cells ectopically expressing either mLSR, mILDR1 or mILDR2 and of HeLa cells transfected with an empty vector (EV) only. Suspensions of transfected HeLa cells (100,000 cells in 1 ml PBS) were incubated for 10 min at RT with 20 nM DyLight488-labeled CDTb (peaks are indicated with black lines). Cells were then washed twice with PBS and finally subjected to FACS analysis. FACS results are presented as histogram plots, where single cell events (cells) are plotted against the intensity of cell surface-bound fluorescence (Log FL int.). White peaks indicate the fluorescence distribution of cells incubated with fluroescence-labeled CDTb and gray peaks represent control cells with no addition of fluorescence-labeled protein.

FIGURE 2. The receptor-binding domain of CDT interacts with the Ig-like domain of LSR. (A) Anti-His immunoblot analysis of the IPTG-induced expression of LSR_{Ig}-His6 in *E. coli*. L, bacterial lysate after cell disruption; SN, supernatant after centrifugation of the bacterial lysate; P, pellet fraction after centrifugation of the bacterial lysate. (B) Enrichment of LSR_{Ig}-His6 from inclusion bodies and verification via SDS-PAGE followed by Coomassie-staining or by immunoblot using an anti-His antibody. (C) GST-pull down assay. GST- or GST-RBD-loaded glutathione beads were incubated with LSR_{Ig}-His6 or without protein. Co-precipitation of LSR_{Ig}-His6 was analyzed by an anti-His immunoblot (top). Equal loading of samples was confirmed via an anti-GST immunoblot (bottom). (D) Surface plasmon resonance binding analysis. LSR_{Ig}-His6 was immobilized on a sensor chip and the binding kinetics of GST or GST-RBD were measured. RU, response units.

FIGURE 3. FACS-based analysis of cell surface-binding of DyLight488-labeled GST-RBD. H1-HeLa(+LSR) (A), CaCo-2 (B), and HCT116 (C) cell suspensions (300,000 cells in 0.1 ml medium) were incubated with increasing concentrations of DyLight488-labeled GST-RBD for 10 min at 4°C before FACS analysis. (D) As shown in (C) but with incubation of the cells with DyLight488-labeled CDTb. Bound fluorescence (FL) is shown relative to the highest value that was set to 100% (n=3, ±SEM). Dotted curve was calculated by SigmaPlot.

FIGURE 4. Knockout of LSR in HCT116 cells via CRISPR-Cas9. (A) Depiction of the base pair insertion (frame-shift mutation) in the LSR knockout cell clone ($HCT116_{\Delta LSR}$) used in this study. Dots indicate identical base pairs compared to $LSR_{Q86X29\text{-}1}$. (B) Anti-LSR immunoblot analysis of whole-cell lysates obtained from HCT116 wild-type (WT) and $HCT116_{\Delta LSR}$ (ΔLSR) cells (top). Equal loading of samples was verified by detecting tubulin with a specific antibody (bottom). (C) Anti-LSR immunoblot analysis of membrane fractions obtained from $HCT116_{\Delta LSR}$ cells transduced with FLAG- or FLAG-LSR retroviruses (top). Equal loading of samples was verified by detecting ATP1A1 (sodium/potassium-transporting ATPase subunit alpha-1) with a specific antibody (bottom). (D) CDT intoxication of HCT116 wild-type (WT) and LSR knockout cells (ΔLSR) and of FLAG- or FLAG-LSR-transduced $HCT116_{\Delta LSR}$ cells. Following a 24 h treatment of the cells with toxin (4 nM CDTa/5 nM CDTb) at 37°C, cell morphology was analyzed microscopically. (E) FACS-based analysis of the binding of DyLight488-labeled GST-RBD to the cell surface of HCT116 wild-type (WT) and LSR knockout cells (ΔLSR) and of FLAG- or FLAG-LSR-transduced $HCT116_{\Delta LSR}$ cells. Cell suspensions (300,000 cells in 0.1 ml medium) were incubated for 10 min at 4°C with 2 µM DyLight488-labeled GST-RBD. Cells were then washed twice with medium and finally subjected to FACS analysis. FACS results are presented as histogram plots, where single cell events (cells) are plotted against the intensity of cell surface-bound fluorescence (Log FL int.). White peaks indicate the fluorescence distribution of cells incubated with fluroescence-labeled GST-RBD and gray peaks represent control cells with no addition of fluorescence-labeled protein.

Downloaded from http://www.jbc.org/ at Shanghai Information Center for Life Sciences, Chinese Academy of Sciences on May 25, 2015

FIGURE 5. LSR splice variants identified in HCT116 cells. (A) Schematic representation of the domain architecture of LSR isoforms identified in HCT116 cells, in direct comparison to isoforms 1 to 6 of LSR with the UniProt accession number Q86X29 and the LSR variant with the GenBank accession number AAH04381.2. TH, transmembrane helix; CR, cysteine-rich region. Greek symbols indicate amino acid insertions or deletions (α: deletion of glutamate-386, β: insertion of an arginine residue between amino acids 519 and 520, γ: deletion of histidine-607, δ: deletion of lysine-637; amino acid numbering refers to LSR_{Q86X29} isoform 1). (B) Isoform-3- and isoform-5-like LSR variants obtained from a HCT116 cDNA library were co-expressed as Tomato- ($LSR_{isoform\text{-}3\text{-}like}$-Tomato) or EGFP-fused ($LSR_{isoform\text{-}5\text{-}like}$-EGFP) proteins HCT116 LSR knockout cells, prior to analysis of their subcellular localization via confocal fluorescence microscopy. Fluorescence images were obtained 48 hours after co-transfection of the cells with the corresponding plasmids. (C) $LSR_{isoform\text{-}5\text{-}like}$-EGFP shown in (B) was co-expressed in HCT116 LSR knockout cells together with cal-dsRed2, an endoplasmic reticulum marker. Confocal images were obtained 2 days after transfection of the cells with the respective plasmids. Scale bar represents 10 µm. mag., magnified area.

FIGURE 6. Generation and ectopic expression of LSR truncations in $HCT116_{\Delta LSR}$ cells. (A) Schematic representation of the truncated LSR versions, either C-terminally fused to EGFP or Tomato (EGFP/Tomato). TH, transmembrane helix; CR, cysteine-rich region. (B) Anti-EGFP (top) and anti-LSR (middle) immunoblot analysis of membrane fractions obtained from HCT116 wild-type (WT) and LSR knockout cells (ΔLSR) and of transfected $HCT116_{\Delta LSR}$ cells ectopically expressing LSR-EGFP, $LSR_{1\text{-}240}$-EGFP or $LSR_{\Delta CR}$-EGFP. Equal loading of samples was verified by detecting ATP1A1 (sodium/potassium-transporting ATPase subunit alpha-1) with a specific antibody (bottom). Open triangles in the anti-LSR immunoblot indicate bands representing endogenous LSR (WT) and LSR fusion proteins, respectively. (C) Analysis of cell surface exposure of Tomato-fused LSR truncations. $HCT116_{\Delta LSR}$ cells were transfected with plasmids encoding LSR-Tomato, $LSR_{1\text{-}240}$-Tomato or $LSR_{\Delta CR}$-Tomato. The following day, cells were detached and the cell suspensions (100,000 cells in 0.5 ml PBS/1% BSA) incubated without or with 20 nM DyLight488-labeled GST-RBD (RBD_{DL488}) for 10 min at 4°C prior to FACS analysis. The upper row represents the red fluorescence (Log FL red) vs. side scatter (SSC) dot plots of the transfected cells. Dots in region 1 (R1) represent non-transfected cells and dots in region 2 (R2) the transfected cells exhibiting a higher red fluorescence. The middle and lower rows represent the green fluorescence (Log FL green) vs. SSC dot plots of the regions R1 and R2, respectively.

FIGURE 7. CDT intoxication of $HCT116_{\Delta LSR}$ cells ectopically expressing LSR-EGFP, $LSR_{1\text{-}240}$-EGFP, and $LSR_{\Delta CR}$-EGFP. One day after transfection of $HCT116_{\Delta LSR}$ cells with the respective plasmids, cells were intoxicated for 3 hours with CDT at 37°C. Intoxication of transfected and non-transfected cells was followed by TRITC-phalloidin staining of actin and confocal fluorescence microscopy to visualize toxin-induced actin depolymerisation (left panel) and by analyzing the effects of the toxin on the cell morphology via differential interference contrast (DIC) microscopy (right panel). Scale bars: 10 µm.

FIGURE 8. Generation of N- and C-terminal RBD truncations and analysis of their binding to LSR. (A) Schematic representation of the different RBD truncations generated in this study. Gray, hatched area indicates the truncated part of the RBD. (B) GST-pull down assay. Glutathione beads loaded with GST alone (GST), GST-RBD (RBD) or the GST-RBD truncations RBD/Δ10C and RBD/Δ80N (upper panel) or RBD/Δ20C and RBD/Δ120N (lower panel), respectively, were incubated with LSR_{Ig}-His6 or without protein. Co-precipitation of LSR_{Ig}-His6 was analyzed by an anti-His immunoblot. (C, D) FACS competition experiments. RBD_{DL488} was incubated with H1-HeLa(+LSR) cell suspensions either alone (1:0) or together with 1- (1:1), 10- (1:10) or 100-fold (1:100) molar excess of non-labeled (D) N- or (C) C-terminal truncations of RBD. Bound fluorescence is shown relative to the mean fluorescence values of samples without competing protein (1:0) that were set to 100% (n = 3, ±SEM).

Downloaded from http://www.jbc.org/ at Shanghai Information Center for Life Sciences, Chinese Academy of Sciences on May 25, 2015

FIGURE 9. Generation of RBD mutants by transposon-based, random mutagenesis and analysis of their binding to LSR. (A) Graphic depiction and sequence comparison of the positions in GST-RBD where the 5-amino acid insertions (T1-T8) were randomly introduced by transposon-based mutagenesis. The numbering of the amino acids of RBD is based on the CDTb full-length protein. (B) Comparison of the purity and stability of wild-type RBD and mutant RBD proteins (T1-T8) via SDS-PAGE and Coomassie staining (3 μg total protein per lane). Arrow indicates the GST-tagged fusion proteins. M, protein molecular-weight marker. (C) FACS competition experiments. RBD_{DL488} was incubated with H1-HeLa(+LSR) cell suspensions either alone (1:0) or together with 1- (1:1), 10- (1:10) or 100-fold (1:100) molar excess of non-labeled RBD or RBD mutants (T1-T8). Bound fluorescence is shown relative to the mean fluorescence values of samples without competing protein (1:0) that were set to 100% ($n \geq 3$, ±SEM). (D) Limited tryptic proteolysis. 5 μg of purified RBD or the RBD mutant T2 were incubated for 10 min at 4°C with increasing concentrations of trypsin (as indicated), followed by SDS-PAGE and Coomassie staining. Arrow indicates the GST-tagged fusion proteins. Asterisk indicates tryptic fragments of RBD and the RBD mutant T2. M, protein molecular-weight marker.

Downloaded from http://www.jbc.org/ at Shanghai Information Center for Life Sciences, Chinese Academy of Sciences on May 25, 2015

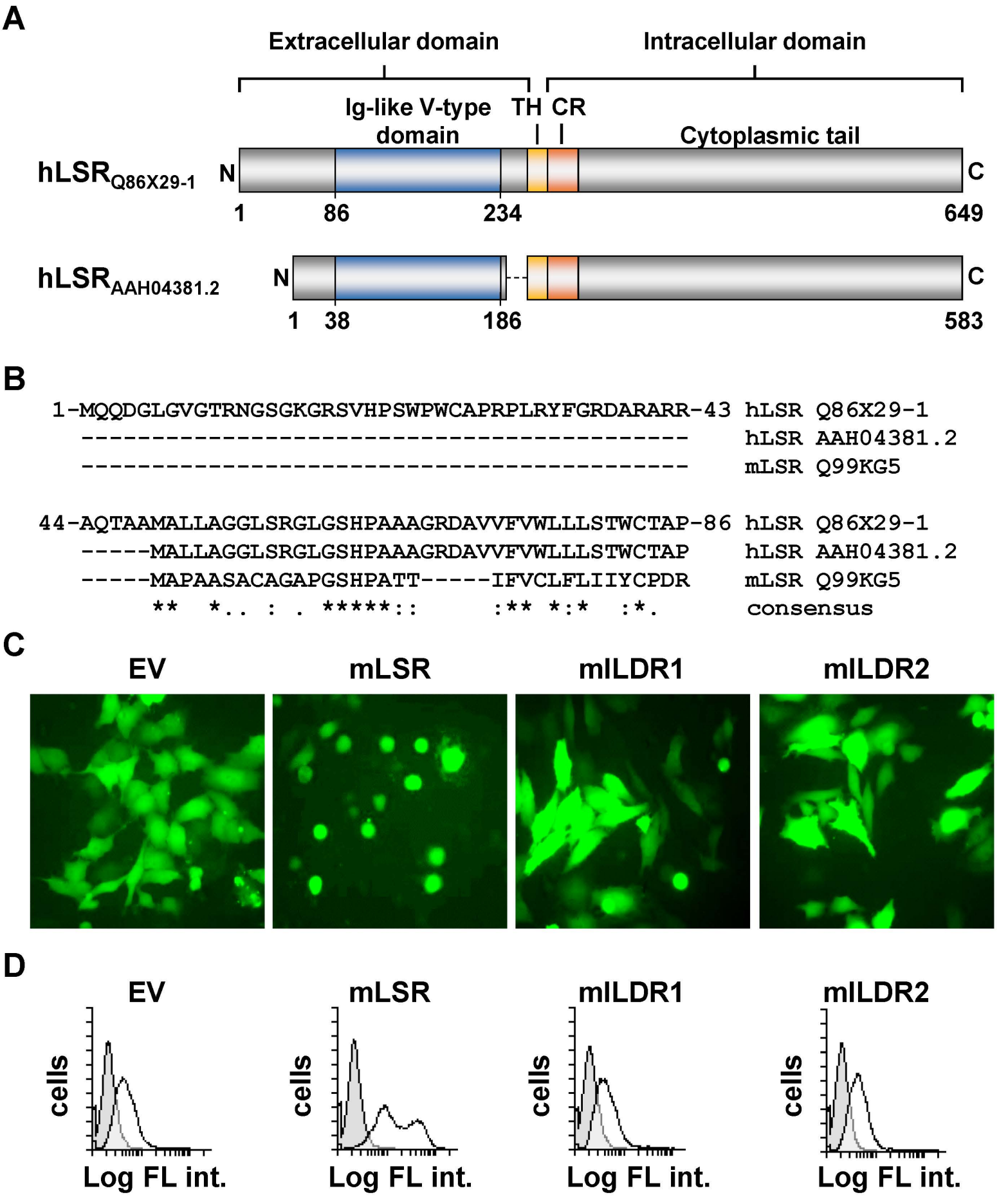

A
Extracellular domain
Intracellular domain
Ig-like V-type domain
TH
CR
Cytoplasmic tail
hLSR Q86X29-1
N
C
1
86
234
649
hLSR AAH04381.2
N
C
1
38
186
583
B
1-MQQDGLGVGTRNGSGKGRSVHPSWPWCAPRPLRYFGRDARARR-43 hLSR Q86X29-1
---------- hLSR AAH04381.2
---------- mLSR Q99KG5
44-AQTAAMALLAGGLSRGLGSHPAAAGRDAVVFVWLLLSTWCTAP-86 hLSR Q86X29-1
-----MALLAGGLSRGLGSHPAAAGRDAVVFVWLLLSTWCTAP hLSR AAH04381.2
-----MAPAASACAGAPGSHPATT-----IFVCLFLIIYCPDR mLSR Q99KG5
** *.. : . *****:: :** *:* :*. consensus
C
EV
mLSR
mILDR1
mILDR2
D
EV
mLSR
mILDR1
mILDR2
cells
Log FL int.

Fig. 1

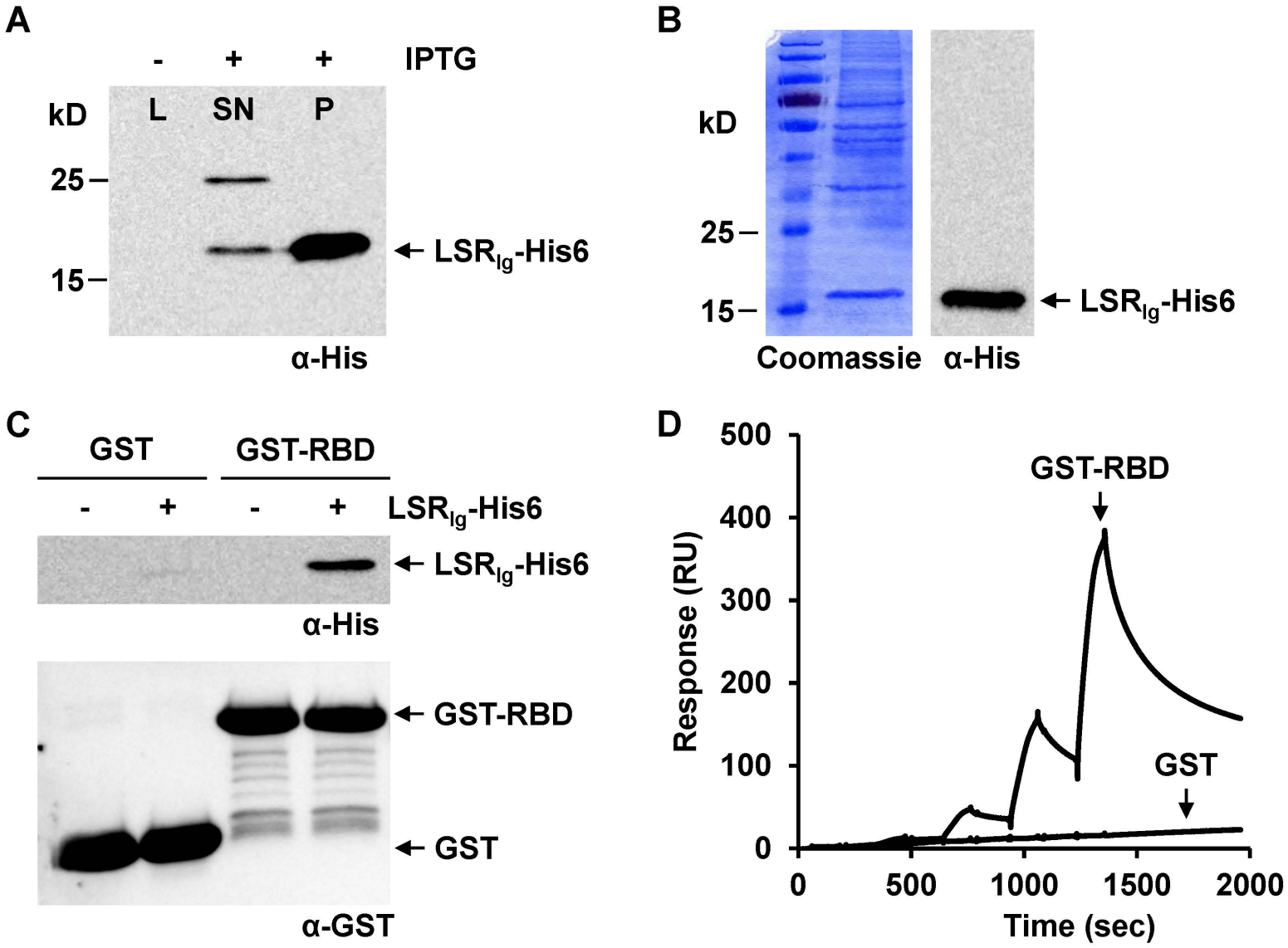

A
- + + IPTG
kD L SN P
25
15
LSRlg-His6
α-His
B
kD
25
15
LSRlg-His6
Coomassie α-His
C
GST GST-RBD
- + - + LSRlg-His6
LSRlg-His6
α-His
GST-RBD
GST
α-GST
D
Response (RU)
500
400
300
200
100
0
GST-RBD
GST
0 500 1000 1500 2000
Time (sec)

Fig. 2

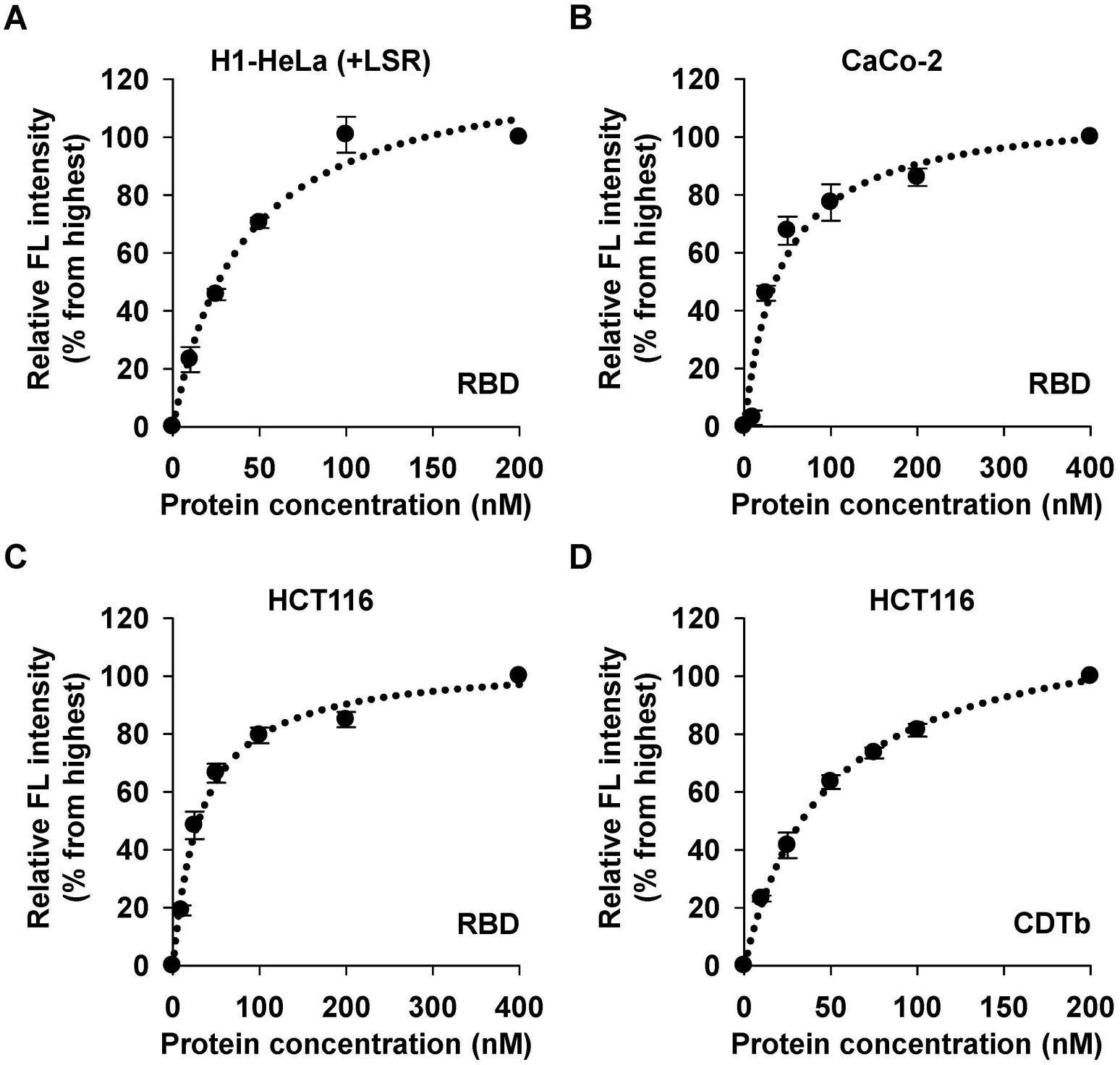

A
H1-HeLa (+LSR)
Relative FL intensity (% from highest)
120
100
80
60
40
20
0
RBD
0
50
100
150
200
Protein concentration (nM)
B
CaCo-2
Relative FL intensity (% from highest)
120
100
80
60
40
20
0
RBD
0
100
200
300
400
Protein concentration (nM)
C
HCT116
Relative FL intensity (% from highest)
120
100
80
60
40
20
0
RBD
0
100
200
300
400
Protein concentration (nM)
D
HCT116
Relative FL intensity (% from highest)
120
100
80
60
40
20
0
CDTb
0
50
100
150
200
Protein concentration (nM)

Fig. 3

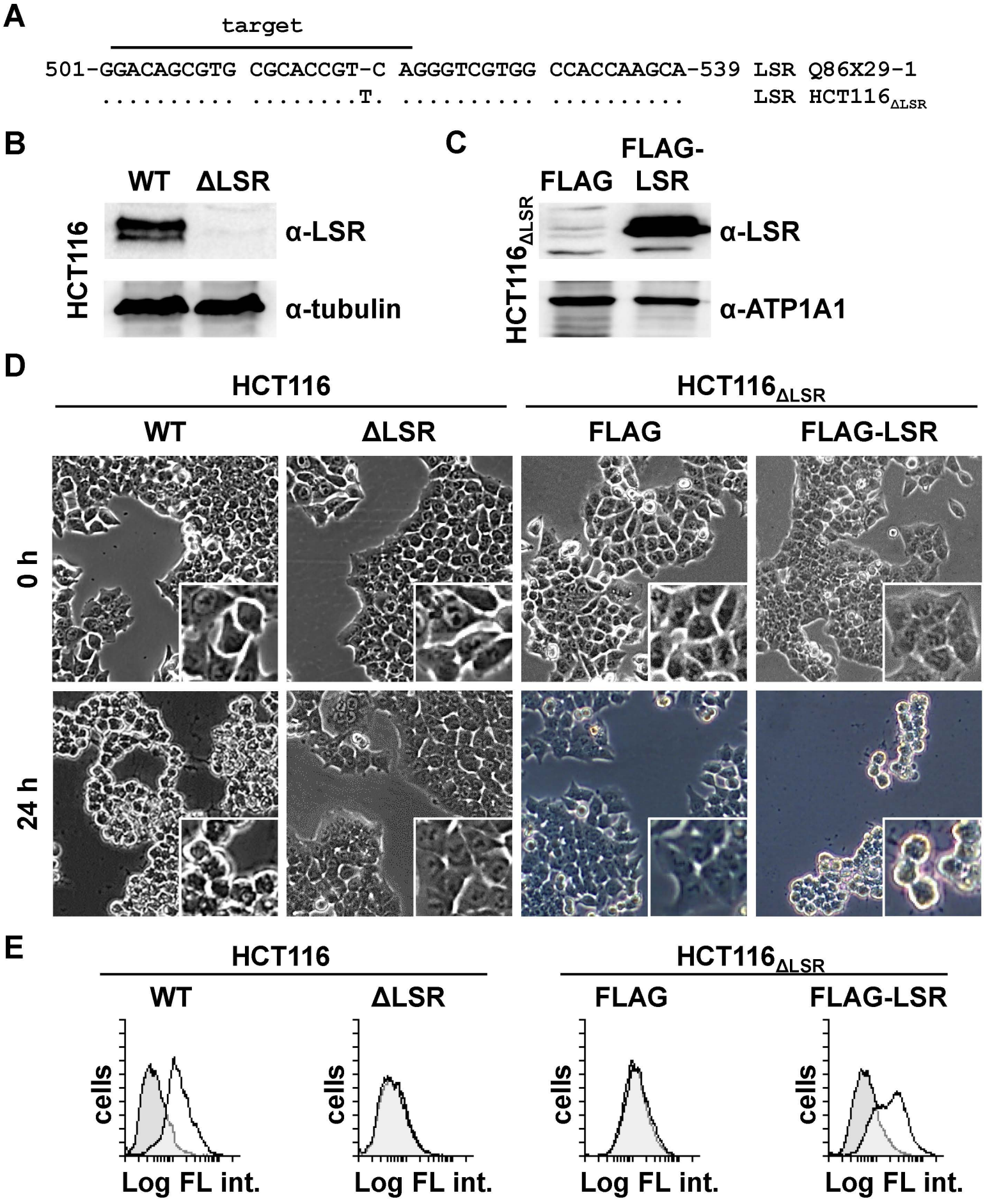

A
target
501-GGACAGCGTG CGCACCGT-C AGGGTCGTGG CCACCAAGCA-539 LSR Q86X29-1
....T. .... LSR HCT116ΔLSR
B
WT
ΔLSR
HCT116
α-LSR
α-tubulin
C
FLAG
FLAG-LSR
HCT116ΔLSR
α-LSR
α-ATP1A1
D
HCT116
HCT116ΔLSR
WT
ΔLSR
FLAG
FLAG-LSR
0 h
24 h
E
HCT116
HCT116ΔLSR
WT
ΔLSR
FLAG
FLAG-LSR
cells
Log FL int.

Fig. 4

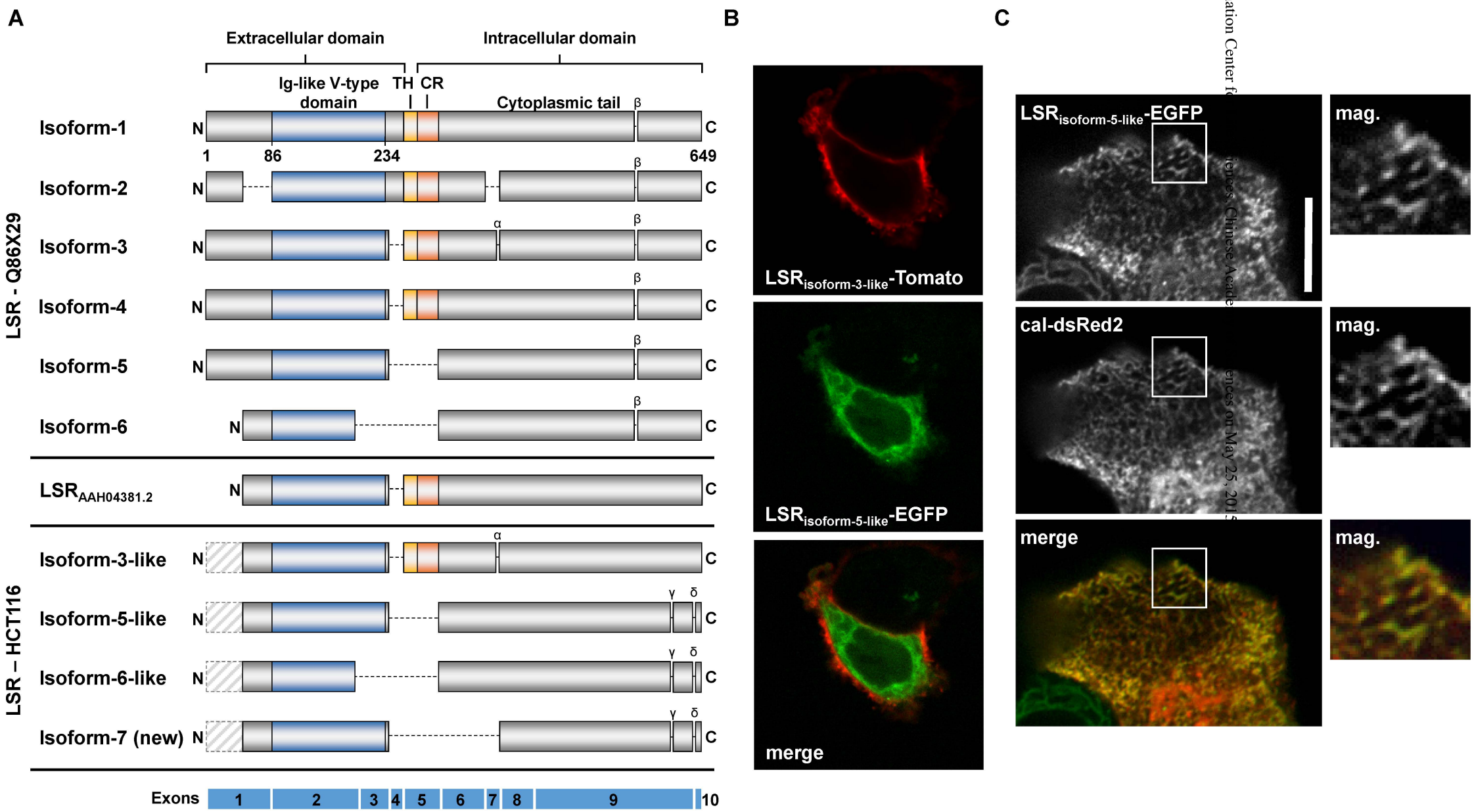

A
Extracellular domain
Intracellular domain
Ig-like V-type domain
TH
CR
Cytoplasmic tail
Isoform-1
Isoform-2
Isoform-3
Isoform-4
Isoform-5
Isoform-6
LSR - Q86X29
LSR$_{AAH04381.2}$
Isoform-3-like
Isoform-5-like
Isoform-6-like
Isoform-7 (new)
LSR – HCT116
N
C
1
86
234
649
α
β
γ
δ
Exons
1
2
3
4
5
6
7
8
9
10
B
LSR$_{isoform-3-like}$-Tomato
LSR$_{isoform-5-like}$-EGFP
merge
C
LSR$_{isoform-5-like}$-EGFP
cal-dsRed2
merge
mag.
mag.
mag.

Fig. 5

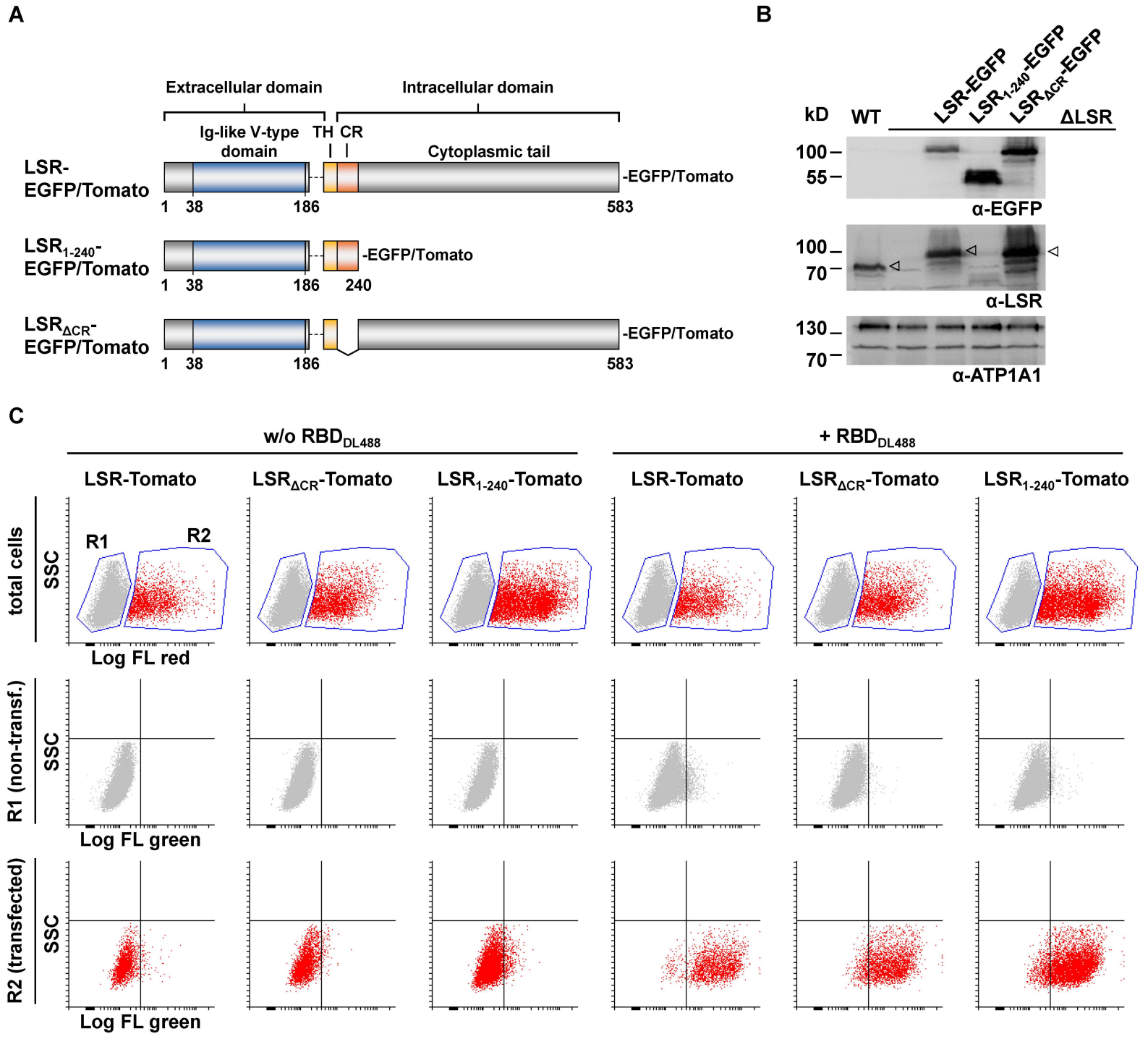

A
Extracellular domain
Intracellular domain
Ig-like V-type domain
TH
CR
Cytoplasmic tail
LSR-EGFP/Tomato
-EGFP/Tomato
1
38
186
583
LSR1-240-EGFP/Tomato
240
LSRΔCR-EGFP/Tomato
B
kD
WT
LSR-EGFP
LSR1-240-EGFP
LSRΔCR-EGFP
ΔLSR
100
55
α-EGFP
70
α-LSR
130
α-ATP1A1
C
w/o RBDDL488
+ RBDDL488
LSR-Tomato
LSRΔCR-Tomato
LSR1-240-Tomato
total cells
SSC
R1
R2
Log FL red
R1 (non-transf.)
Log FL green
R2 (transfected)

Fig. 6

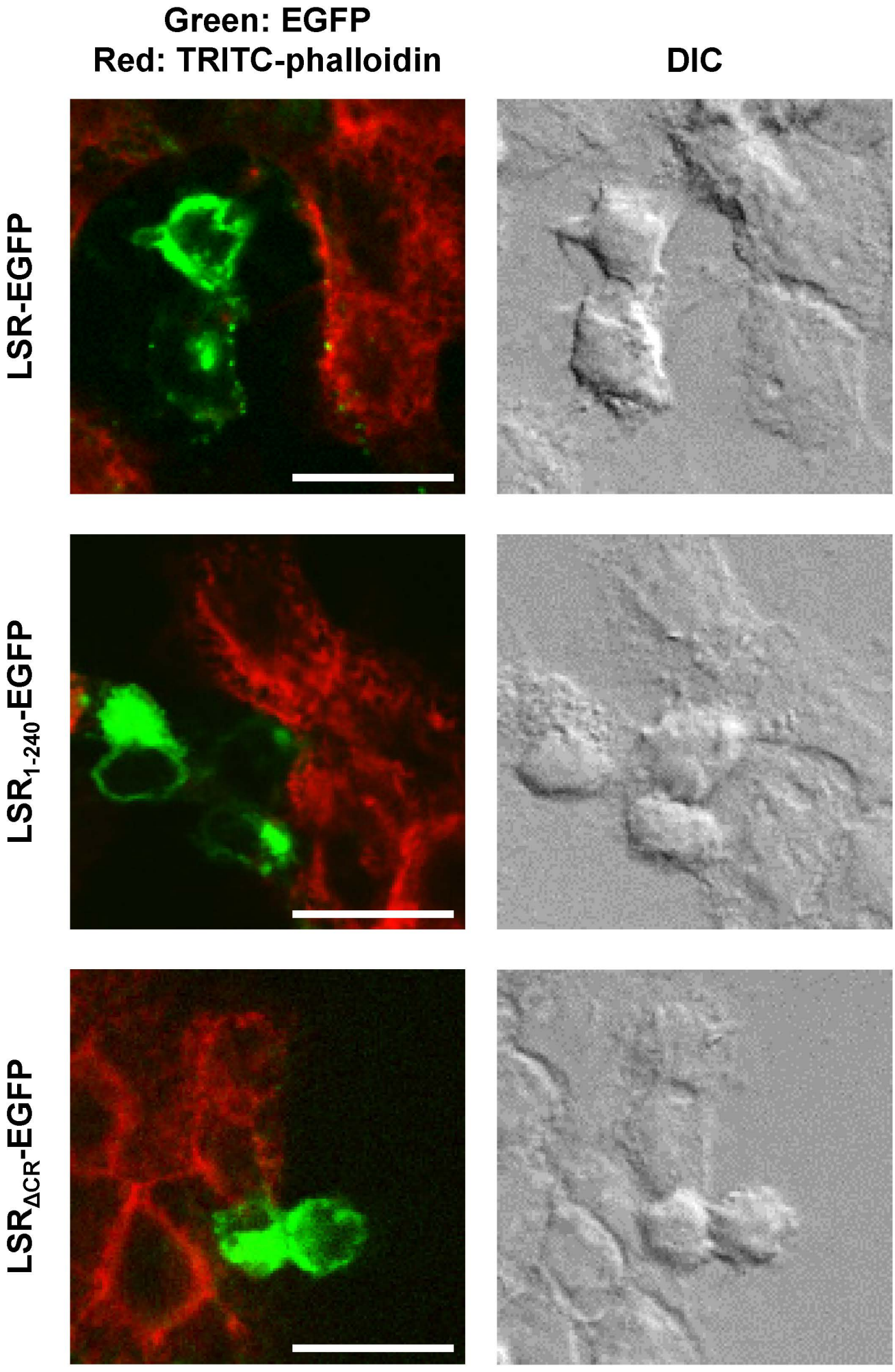

Green: EGFP
Red: TRITC-phalloidin
DIC
LSR-EGFP
LSR1-240-EGFP
LSRΔCR-EGFP

Fig. 7

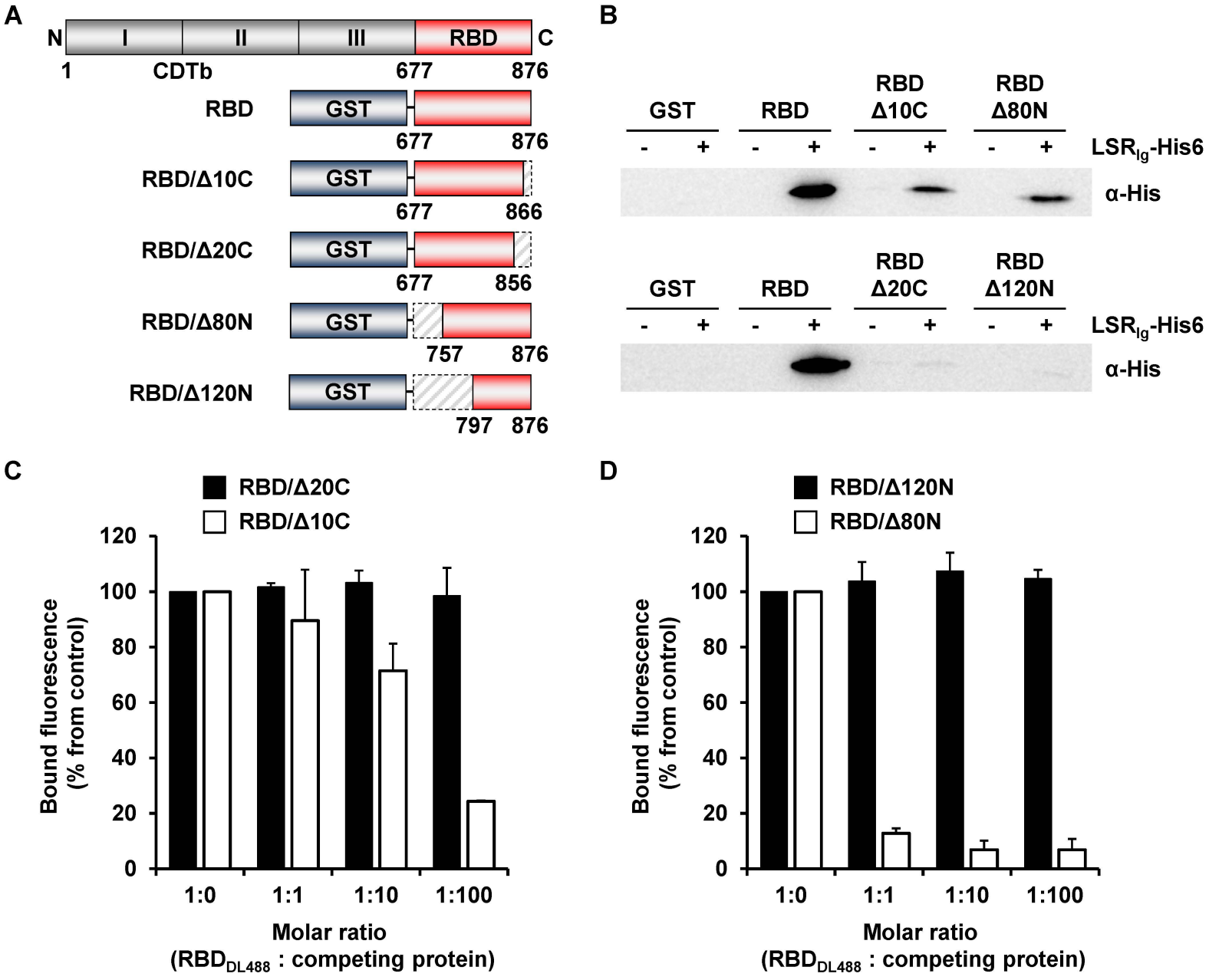

A
N
I
II
III
RBD
C
1
CDTb
677
876
RBD
GST
677
876
RBD/Δ10C
GST
677
866
RBD/Δ20C
GST
677
856
RBD/Δ80N
GST
757
876
RBD/Δ120N
GST
797
876
B
GST
RBD
RBD Δ10C
RBD Δ80N
- + - + - + - +
LSR$_{Ig}$-His6
α-His
GST
RBD
RBD Δ20C
RBD Δ120N
- + - + - + - +
LSR$_{Ig}$-His6
α-His
C
RBD/Δ20C
RBD/Δ10C
Bound fluorescence (% from control)
120
100
80
60
40
20
0
1:0
1:1
1:10
1:100
Molar ratio
(RBD$_{DL488}$: competing protein)
D
RBD/Δ120N
RBD/Δ80N
Bound fluorescence (% from control)
120
100
80
60
40
20
0
1:0
1:1
1:10
1:100
Molar ratio
(RBD$_{DL488}$: competing protein)

Fig. 8

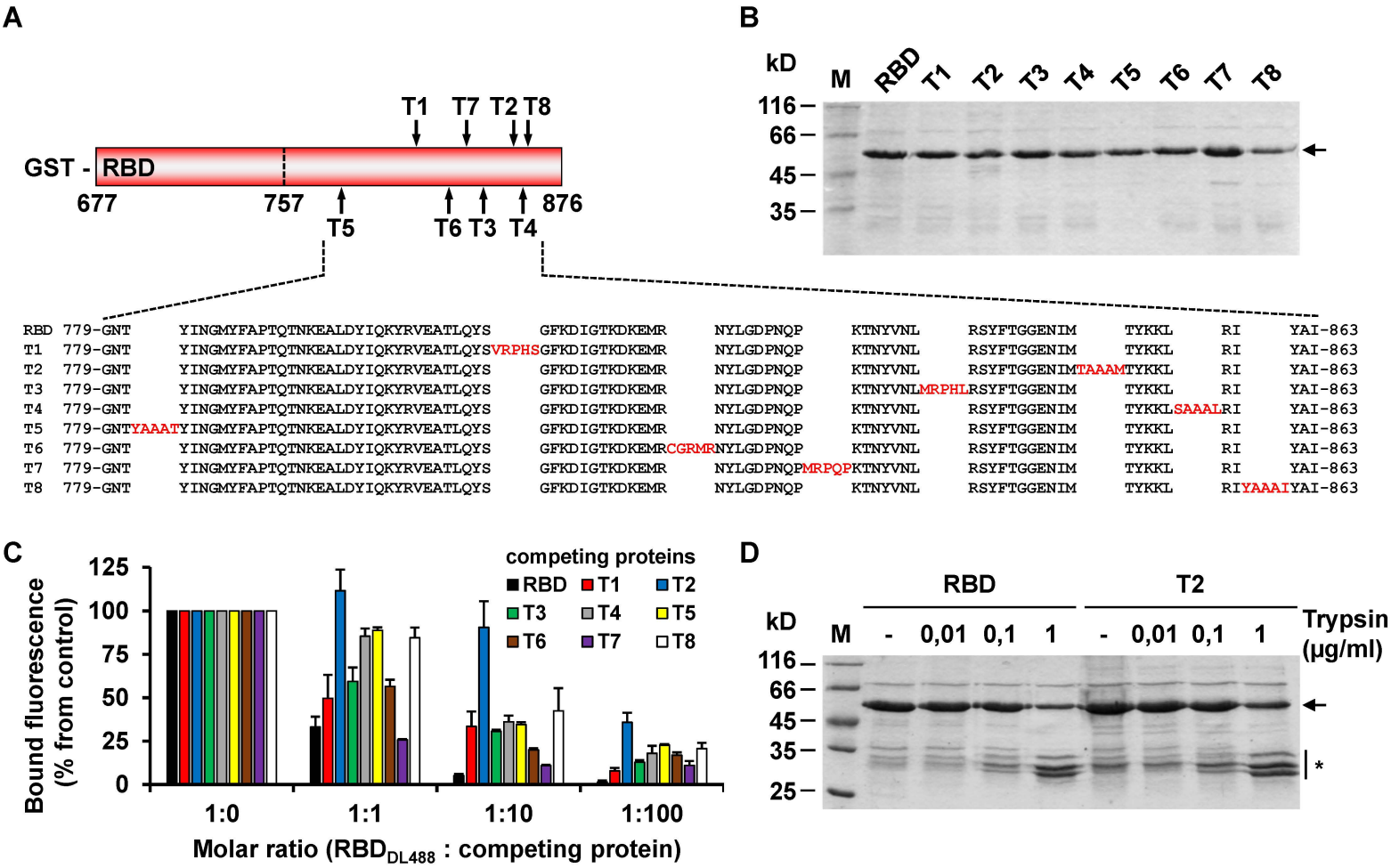

A
T1 T7 T2 T8
GST - RBD
677
757
876
T5
T6 T3 T4
RBD 779-GNT YINGMYFAPTQTNKEALDYIQKYRVEATLQYS GFKDIGTKDKEMR NYLGDPNQP KTNYVNL RSYFTGGENIM TYKKL RI YAI-863
T1 779-GNT YINGMYFAPTQTNKEALDYIQKYRVEATLQYSVRPHSGFKDIGTKDKEMR NYLGDPNQP KTNYVNL RSYFTGGENIM TYKKL RI YAI-863
T2 779-GNT YINGMYFAPTQTNKEALDYIQKYRVEATLQYS GFKDIGTKDKEMR NYLGDPNQP KTNYVNL RSYFTGGENIMTAAAMTYKKL RI YAI-863
T3 779-GNT YINGMYFAPTQTNKEALDYIQKYRVEATLQYS GFKDIGTKDKEMR NYLGDPNQP KTNYVNLMRPHLRSYFTGGENIM TYKKL RI YAI-863
T4 779-GNT YINGMYFAPTQTNKEALDYIQKYRVEATLQYS GFKDIGTKDKEMR NYLGDPNQP KTNYVNL RSYFTGGENIM TYKKLSAAALRI YAI-863
T5 779-GNTYAAATYINGMYFAPTQTNKEALDYIQKYRVEATLQYS GFKDIGTKDKEMR NYLGDPNQP KTNYVNL RSYFTGGENIM TYKKL RI YAI-863
T6 779-GNT YINGMYFAPTQTNKEALDYIQKYRVEATLQYS GFKDIGTKDKEMRCGRMRNYLGDPNQP KTNYVNL RSYFTGGENIM TYKKL RI YAI-863
T7 779-GNT YINGMYFAPTQTNKEALDYIQKYRVEATLQYS GFKDIGTKDKEMR NYLGDPNQPMRPQPKTNYVNL RSYFTGGENIM TYKKL RI YAI-863
T8 779-GNT YINGMYFAPTQTNKEALDYIQKYRVEATLQYS GFKDIGTKDKEMR NYLGDPNQP KTNYVNL RSYFTGGENIM TYKKL RIYAAAIYAI-863
B
kD
M
RBD
T1
T2
T3
T4
T5
T6
T7
T8
116
66
45
35
C
competing proteins
RBD
T1
T2
T3
T4
T5
T6
T7
T8
Bound fluorescence (% from control)
125
100
75
50
25
0
1:0
1:1
1:10
1:100
Molar ratio (RBDDL488 : competing protein)
D
RBD
T2
kD
M
-
0,01
0,1
1
-
0,01
0,1
1
Trypsin (µg/ml)
116
66
45
35
25
*

Fig. 9



Microbiology:

Interaction of the *Clostridium difficile* Binary Toxin CDT and its Host Cell Receptor LSR



Sarah Hemmasi, Bernd A. Czulkies, Björn Schorch, Antonia Veit, Klaus Aktories and Panagiotis Papatheodorou

J. Biol. Chem. published online April 16, 2015

Access the most updated version of this article at doi: 10.1074/jbc.M115.650523

Find articles, minireviews, Reflections and Classics on similar topics on the JBC Affinity Sites.

Alerts:
- When this article is cited
- When a correction for this article is posted

Click here to choose from all of JBC's e-mail alerts

This article cites 0 references, 0 of which can be accessed free at
http://www.jbc.org/content/early/2015/04/16/jbc.M115.650523.full.html#ref-list-1

Downloaded from http://www.jbc.org/ at Shanghai Information Center for Life Sciences, Chinese Academy of Sciences on May 25, 2015